Recent Advances in Research and Forecasting of Tropical Cyclone Rainfall

Kevin Cheung[1], Zifeng Yu[2], Russell L. Elsberry[3], Michael Bell[4], Haiyan Jiang[5], Tsz Cheung Lee[6], Kuo-Chen Lu[7], Yoshinori Oikawa[8], Liangbo Qi[9], Robert F. Rogers[10], Kazuhisa Tsuboki[11]

[1]Macquarie University, Australia

[2]Shanghai Typhoon Institute, China

[3]University of Colorado-Colorado Springs, USA

[4]Colorado State University, USA

[5]Florida International University, USA

[6]Hong Kong Observatory, Hong Kong

[7]Pacific Science Association

[8]RSMC Tokyo/Japan Meteorological Agency, Japan

[9]Shanghai Meteorological Service, China

[10]NOAA/AOML/Hurricane Research Division, USA

[11]Nagoya University, Japan

February 2018
Tropical Cyclone Research and Review
Special Issue

Corresponding Author: Kevin Cheung, Department of Environmental Sciences
Macquarie University, North Ryde, NSW 2109, Australia
Email: kevin.cheung@mq.edu.au

Abstract

In preparation for the Fourth International Workshop on Tropical Cyclone Landfall Processes (IWTCLP-IV), a summary of recent research studies and the forecasting challenges of tropical cyclone (TC) rainfall has been prepared. The extreme rainfall accumulations in Hurricane Harvey (2017) near Houston, Texas and Typhoon Damrey (2017) in southern Vietnam are examples of the TC rainfall forecasting challenges. Some progress is being made in understanding the internal rainfall dynamics via case studies. Environmental effects such as vertical wind shear and terrain-induced rainfall have been studied, as well as the rainfall relationships with TC intensity and structure. Numerical model predictions of TC-related rainfall have been improved via data assimilation, microphysics representation, improved resolution, and ensemble quantitative precipitation forecast techniques. Some attempts have been made to improve the verification techniques as well. A basic forecast challenge for TC-related rainfall is monitoring the existing rainfall distribution via satellite or coastal radars, or from over-land rain gauges. Forecasters also need assistance in understanding how seemingly similar landfall locations relative to the TC experience different rainfall distributions. In addition, forecasters must cope with anomalous TC activity and landfall distributions in response to various environmental effects.

1. Introduction

Rainfall associated with a tropical cyclone (TC) is one of the most severe impacts to the coastal regions where the storms make landfall. Heavy rainfall from TCs not only causes flash floods at the coast but may also bring torrential rain far inland from the coast. Climatologically, TC rainfall contributes significantly to the total and extreme precipitation events in all global regions where TC landfalls occur. Based on satellite precipitation estimates, TCs account for an average of 3.5% ± 1% of the total number of rainy days over land areas that experience cyclonic activity regardless of the basin considered, and TC days represent between 13% and 31% of daily extremes above 4 inches (~102 mm) per day (Prat and Nelson 2016). In terms of extremes (as observed by rain gauges), the largest TC-induced rainfall totals occur in East Asia (>400 mm/year) and northeastern Australia (>200 mm/year), and then in the southeastern United States and along the coast of the Gulf of Mexico (100–150 mm/year) (Khouakhi et al. 2017). Using annual maximum and peak-over-threshold approaches, Khouakhi et al. (2017) also found that the highest proportions of TC-induced rainfall are found in East Asia, followed by Australia and North and Central America.

Two TC landfall cases last year illustrate the severity and forecast challenge associated with rainfall events. One case is Hurricane Harvey (2017) that made landfall in Texas, US in late August. Another one is Typhoon Damrey (2017) that made landfall in southern Vietnam in early November. Both TCs caused record-breaking precipitation at their landfall regions. Widespread flooding associated with Hurricane Harvey claimed more than 40 deaths and billions of U.S. dollars in property damage. The flooding triggered by Typhoon Damrey led to 89 deaths, with 18 people missing along the south coast of Vietnam. Considering the time for local governments to issue an emergency alert or organize extensive evacuations, accurate rainfall or flooding forecasts have to be provided to decision makers 2-3 days in advance. However, forecasting

rainfall induced by TC landfall for lead times longer than 2 days may be determined by many factors, including the TC track, intensity, and structure, as well as by weather systems in the vicinity. It is well recognized by forecasters that issuing a credible heavy rainfall forecast or warning 2 days in advance is still a highly challenging task.

Since the review reports prepared for the WMO Third International Workshop on Tropical Cyclone Landfall Processes (IWTCLP-III) (Yu 2014, Marchok et al. 2014, and Woo et al. 2014), advances have been made in many aspects of the science and in the forecast techniques of TC rainfall. Some advances for several TC basins have been identified by the working group on TC rainfall and are summarized in this article. This summary will include observation systems, theoretical research and conceptual model developments, forecast techniques, and numerical guidance. Some recent high-impact TC cases will be described that reveal the forecast challenges. Sections 2-7 first discuss studies on regional TC rainfall trends, internal dynamics and environmental contributions to rainfall, relationships with TC intensity and structure, advances in numerical models, and cases of heavy rainfall remote from the TC center, respectively. Section 8 describes several TC cases that occurred recently that emphasize the importance of synoptic factors to rainfall and anomalous rainfall patterns. The final concluding remarks provide some perspectives for making further advances in research and operations in the next few years.

2. TC Rainfall Climatology and Regional Trends

Rainfall from TCs, which are some of the major convective systems in the tropics, contribute significantly to the annual rainfall amounts in a number of regions around the globe. When TCs migrate to higher latitudes, their structure may change but often they still pose a threat for heavy rainfall. For example, extratropical transitions of hurricanes may affect the

European region, and recurvature migration of TCs in the South Pacific may lead to intense low pressure systems in the midlatitude eastern Australian region. Thus, contributions of TCs to extreme rainfall are not limited to the tropics. The global TC rainfall climatology was previously documented by Yu (2014) in the IWTC-III report, and regional climatologies for the U.S., Australia, China, and Taiwan were provided. The recent global studies of Prat and Nelson (2016) and Khouakhi et al. (2017) have been mentioned in the Introduction. Some regional updates since 2014 will be provided below. These regional studies illustrate the rainfall variability due to TC tracks and rainband structure, adjacent synoptic systems, and environmental interactions. Regional trends of TC versus non-TC rainfall may differ in magnitude and even in the sign of the change due to the effects of the urbanization and climate changes.

a. East Asia

Chen and Fu (2015) analyzed the monthly, seasonal, and annual contributions of TC rainfall over East Asia associated with western North Pacific (WNP) TCs based on the TRMM 3B42 multi-satellite precipitation analyses. Chen and Fu (2015) found that TC seasonal rainfall contribution ranges from 4% in inland regions to above 40% in ocean regions. On monthly timescales, TCs regionally may contribute 60% to the total rainfall during the entire TC season. The largest contributions of TC rainfall occurred in August (28%) over the ocean and in December (23%) over land. The maximum annual contribution of TC rainfall was in 2004 over the ocean (30%) and in 1998 over the land (20%).

Li et al. (2015) examined the climatological TC-related rainfall in Hong Kong in relation to several TC parameters, and then investigated the trends in TC rainfall, non-TC rainfall, and total rainfall during the past few decades. On average, rainfall in Hong Kong induced by TCs can account for about 25% of the total precipitation during summer and fall, and the contribution

can be even larger in extreme cases. Composite analyses suggest that extreme TC rainfall is often related to TCs that are in close proximity to Hong Kong, have higher intensities, and are associated with stronger convection and moisture convergence in the vicinity of Hong Kong. Observed trends of different rainfall indices suggest that the rainfall variability in Hong Kong is considerably affected by the TC rainfall, which has a decreasing trend in frequency and intensity in recent decades. However, there is an increasing trend in daily rainfall frequency and intensity for non-TC rainfall in Hong Kong.

Guo et al. (2017) examined the rainfall and moisture transports related to TCs in the coastal region of East Asia (EA). In addition, the contribution of TCs to the regional water budget is compared with other contributors, and especially the mean circulation of the EA summer monsoon (EASM). Based on ERA-Interim reanalysis (1979–2012), the trajectories of TCs are identified using an objective feature tracking method. During July to October (JASO, in which over 60% of TCs occur), TC rainfall contributes10%–30% of the monthly total rainfall over the coastal region of EA, with the largest contribution over the south/southeast coast of China during September. The TCs have the largest contributions to extreme daily rainfall (above the 95th percentile), with 50%–60% contributions over the EA coast and as high as 70% over Taiwan Island. TCs transport less moisture over EA than the mean EASM. During the September peak in the seasonal cycle of TCs, the moisture transported primarily by westward-moving TCs is an important source for the water budget over the EA region because the EASM is withdrawing during September.

b. The Philippines

Bagtasa (2017) combined ground and satellite observations of TC-induced rainfall in the Philippines to produce a 64-y precipitation dataset. A total of 1673 TCs were examined using best-

track data from the Japan Meteorological Agency (JMA), and all rainfall within 10° degree latitude/longitude (~1110 km) of the TC center was considered to be TC-induced rainfall. TC rain contribution is highest (54%) along the western coast of Luzon and lowest (6%) in the southern islands of Mindanao. This largest TC rain contribution is attributed to an enhancement of the Asian southwest monsoon when the TCs are located to the northeast of the Philippines.

c. Mexico

Breña-Naranjo et al. (2015) analyzed TC rainfall using both space-borne and ground-based observation data. While the annual total rainfall in Mexico is weakly related (0-20%) to the contribution by TCs, the lower Baja California Peninsula receives on average ~40% (and up to 80%) of its total annual rainfall from TCs. Indeed, southern regions of Mexico can receive more than 2400 mm of rainfall during years with significant TC activity.

d. Australia

Villarini and Dennistone (2016) analyzed extreme TC rainfall based on over 2000 rain gauges in Australia and found that TCs play a prominent role in extreme rainfall over much of Australia. For example, more than half of the largest annual rainfall events are associated with TCs over the coastal regions, and in particular over Western Australia. Moreover, the TC fractional contribution to extreme rainfall increases for the largest rainfall events, with approximately 66–100% of annual maxima in excess of 100 mm (~4 inches) at over one third of the locations in Western Australia are associated with TCs.

Ng et al. (2015) also identified a large high fraction of rainfall from TCs in Northwest Australian annual rainfall. At some coastal stations, more than 40% of the rainfall arises from TCs, with the largest fractions occurring in the October through December period. Whereas

some coastal stations receive more than 70% of their rainfall from TCs, a sharp gradient in this percentage is found farther from the coastline, with inland percentages of TC-related rainfall typically less than 30%.

3. Remote Rainfall Events

Bao et al. (2015) studied Typhoon Fitow (2013) that made landfall south of Shanghai, China, on 6 October. During the following two days, precipitation in excess of 300 mm day^{-1} occurred 400 km to the north of the typhoon center. The rain-producing systems included outward-spiraling rainbands, which developed in the storm's northern sector in favorable environmental vertical wind shear, and frontal clouds as a result of coastal frontogenesis (**Fig. 1**). In addition to enhanced ascent over the rain area, there were increases in low-level moisture, convective instability, and mid-level cyclonic relative vorticity. There is evidence of a pre-conditioning period prior to the rain when mid-level subsidence and boundary layer moistening occurred. Analyses of low-level equivalent potential temperature indicated a cold, dry airstream wrapped into Fitow's circulation from the north after landfall, which limited the inner-core rainfall and produced a cold-air boundary. However, an extended warm, moist airstream from the east converged with the cold-air intrusion that then led to the heavy rain. In addition, the large-scale flow reorganized as anticyclones developed over China and the North Pacific. At upper levels, a large-amplitude trough relocated over central China with an entrance to the southwesterly jet positioned near Shanghai. Back trajectories from the rain area indicate that four environmental interactions developed: (i) increasing mid-level injection of moist potential vorticity (PV) from Fitow's circulation; (ii) low-level warm, moist inflow from the east; (iii) midlevel inflow from nearby Typhoon Danas; and (iv) decreasing mid- to upper-level

injection of PV from the midlatitude trough. Bao et al. concluded that the resultant PV structure change provided a very favorable environment for the persistent development of rain systems.

Deng et al. (2017) studied TC Bilis (2006) that had made landfall on the China coast at 0500 UTC 14 July, but sudden and unexpected torrential rain commenced about 7 hours after landfall some 400 km southwest of the weakening circulation center. At least 843 people were killed and the direct economic loss was estimated at up to 5 billion U.S. dollars in this remote rain event.

Even though the vertical vorticity decreased and deformation increased around Bilis's circulation, a strong gradient wind imbalance (GWI) occurred at midlevels in the northwestern quadrant of Bilis. Consequently, a strong airstream with high PV was shifted from the inner circulation to the outer radii. Both backward and forward Lagrangian trajectories indicated this redistribution resulted in an increase of mid-level PV toward the rainfall areas. While this outward transport of mid-level PV is consistent with the rapid decline in rainfall near Bilis's center, large differential horizontal PV advection below 400 hPa occurred over the rainfall area. This advection of high PV over the rainfall areas was associated with a lifting of the local isentropic surfaces and the formation of a cold dome in the mid- to lower-troposphere, which also established favorable conditions for warm advection and ascent over the raised isentropic surfaces. Deng et al. concluded these adiabatic ascent mechanisms released conditional instability and resulted in broadscale convection and heavy rainfall.

Tang et al. (2014) found complex interactions with low-level vertical wind shear led to conditions favorable for a squall-line-type principal rainband in Typhoon Hagupit (2008). This principal rainband in Typhoon Hagupit was more similar to a typical outer rainband versus the overturning-type inner rainband usually associated with the eyewall convection (**Fig. 2**). Analyses

indicated an approximate balance between the low-level vertical wind shear and the horizontal vorticity associated with the cold pool, and interactions with adjacent low-level jets may have also contributed to the intense convection.

Wang et al. (2015) studied a remote rain event between the circulation of Typhoon Morakot (2009) and the southwest monsoon. Wang et al. analyzed reversed vertical wind shear near a low-level jet core. Convective redevelopment, cell merging, and back-building mechanism were identified as contributors to the heavy rainfall associated with Typhoon Morakot that was quite similar to non-TC mesoscale convective systems.

Galarneau (2015) analyzed a predecessor rain event (PRE) on 25 August 2012 over the Straits of Florida ahead of TC Isaac and related this PRE to the TC track changes. This PRE was unique compared to previously documented PREs in midlatitudes because it occurred over the oceanic subtropics and impacted the track of an approaching TC. The Isaac PRE developed in conjunction with a tropical moisture plume with precipitable water values over 60 mm that intersected a region of mid- and upper-level frontogenesis and warm air advection on the southeastern flank of an upper-level trough. The PRE occurred in an environment with more abundant tropical moisture and weaker synoptic-scale forcing for ascent compared to the environments in which midlatitude PREs have typically developed.

The Isaac PRE contributed to the fracture of the upper-level trough through negative potential vorticity advection associated with the convectively-driven, divergent outflow. Fracture of the upper-level trough and mid-level cyclonic vorticity amplification associated with the PRE deflected the track of Isaac south of Florida and into the Gulf of Mexico. Forecasts from the National Centers for Environmental Prediction–Global Forecast System (NCEP–GFS) initialized at 0000 UTC 21–24 August 2012 failed to predict the PRE, and thus the GFS predicted TC Isaac

would recurve over Florida and then move into the eastern Gulf of Mexico rather than a continued northwestward track toward southeast Louisiana. This relationship between the PRE and TC Isaac's track changes was confirmed with a vorticity inversion and detailed diagnosis of the GFS track forecast initialized at 0000 UTC 22 August.

4. Environmental Effects

a. Vertical wind shear

Bell (2017) emphasized that vertical wind shear (VWS) is a primary contributor to the organization of tropical convection, and has one of the largest influences on the TC precipitation distribution as revealed by composites of satellite, airborne Doppler radar, and lightning detection networks (Corbosiero and Molinari 2003, Chen et al. 2006, Reasor et al. 2013). In weak vertical wind shear, the TC eyewall and rainband precipitation are more symmetric around the center, but they become increasingly concentrated downshear and left-of-shear (for Northern Hemisphere storms) as the vertical wind shear increases (Hence and Houze 2012).

Yu et al. (2015) studied rainfall asymmetries utilizing the Tropical Rainfall Measuring Mission (TRMM) satellite 3B42 rainfall estimates in TCs that made landfall in Hainan (HN), Guangdong (GD), Fujian (FJ) and Zhejiang (ZJ) regions of mainland China and Taiwan (TW) from 2001 to 2009. These landfalling TCs generally had a wavenumber-one (WN-1) rainfall asymmetry with a downshear to downshear-left rainfall maximum, which is consistent with previous studies for TCs over the open ocean. Before landfall (**Fig. 3, left column**), the WN-1 rainfall asymmetry at ZJ along the East China coast was cyclonically rotated relative to the asymmetry at HN along the South China coast. At landfall (**Fig. 3, middle column**), the rainfall maximum tends to be rotated from southwest to southeast of the TC center. After landfall (**Fig. 3, right column**), the cyclonic rotation tends to be shifted from southwest to northeast of the TC

center in the five regions ranging from South China to East China. These cyclonic rotations in the location of rainfall maximum are well correlated with a cyclonic rotation in the environmental VWS between 200 hPa and 850 hPa, which indicates that the rainfall asymmetry in TCs that made landfall over China is predominantly controlled by the large-scale VWS. The cyclonic rotation of VWS was found to be related to the different interactions between the mid-latitude westerlies and the landfalling TCs in different regions. As expected, the axisymmetric (WN-0) component of rainfall generally decreases after landfall in most studied regions.

b. Terrain effects

The direct lifting effect by the terrain is only one of many orographic effects on a TC (Houze 2012). The microphysics can be strongly modulated by the flow over the terrain, which results in changes in the dominant rain processes in the upslope versus the downslope flow (DeHart and Houze 2017). Airborne radar data were used by DeHart and Houze to analyze the precipitation of Hurricane Karl (2010), which made landfall along the mountainous terrain of eastern Mexico. In the upslope flow, shallow rainfall enhancement 1-2 km above the surface was due to orographically generated cloud water that was enhanced by raindrop accretion. In the downslope flow, precipitation was dominated by fallstreaks originating above the melting level. DeHart and Houze concluded that orographic modification processes in a landfalling TC are highly dynamic in nature.

5. Relationship with TC Intensity and Structure

Yu et al. (2017) applied TRMM satellite 3B42 rainfall estimates for 133 landfalling TCs over China during 2001-2015 to examine the relationship between TC intensity and rainfall distribution. The rain rate of each TC was decomposed into axisymmetric and asymmetric

components. On average, axisymmetric (WN-0) rainfall is closely related to TC intensity. Higher intensity TCs have larger peak axisymmetric rain, larger averaged total rain, larger averaged rain areas, and larger averaged amplitude of the WN-0 rainfall, but lower amplitude of WN-1, -2, -3, -4 rain relative to the total rainfall. Rapidly-decaying TCs have the most rapid decrease in both the total rainfall and the axisymmetric rainfall relative to the total rain than do intensifying or rapidly intensifying storm categories. However, the maximum total rain, maximum rain area, and maximum rain rate are not highly correlated with TC intensity, which indicates that stronger TCs do not have systematically higher maximum rain rates than weaker storms.

Yu et al. (2017) also show that the translational speed of TCs has little effect on the asymmetric rainfall distribution in landfalling TCs. The maximum rainfall for both the weaker and stronger TCs is generally located downshear and to its left. However, when the environmental VWS is less than 5 m s^{-1}, the asymmetric rainfall maxima are more frequently located upshear and onshore (**Fig. 4**), which suggests that in a weak VWS environment the coastline could have a significant effect on the rainfall asymmetry in landfalling TCs.

Although the intensity guidance of TCs has improved significantly in the past few decades, forecasting the TC intensity change, especially rapid intensification (RI) still remains challenging (DeMaria et al. 2014). Rainfall and convection within the inner-core region of TCs have been linked with RI in several satellite-based observational studies, such as Jiang (2012), Jiang and Ramirez (2013), and Zagrodnik and Jiang (2014). More recently, Tao and Jiang (2015) statistically analyzed shear-relative distributions of four types of precipitation/convection in TCs using 14 years of TRMM Precipitation Radar (PR) data. Tao and Jiang found that increased and widespread shallow precipitation around the storm center is a first sign of RI and may be used as

a predictor of the onset of RI (Fig. 5). The contribution to total volumetric rain and latent heating from shallow and moderate precipitation in the inner core is greater in RI storms than in non-RI storms, while the opposite is true for moderately deep and very deep precipitation. Tao and Jiang thus suggest that RI is more likely triggered by the increase of shallow-to-moderate precipitation, and the appearance of more moderate-to-very deep convection during the RI event is more likely a response or a positive feedback to changes in the vortex intensity.

Using the same TRMM PR dataset, Tao et al. (2017) examined the relative importance of stratiform and convective precipitation with respect to the evolution of RI events. Tao et al. found that the onset of RI follows a significant increase in the occurrence and azimuthal coverage of stratiform rainfall in all shear-relative quadrants, but especially in the upshear-left quadrant. On the other hand, slowly intensifying (SI) storms have a much lower percent stratiform rain occurrence within the inner core (**Fig. 6**). The relatively larger areal coverage of stratiform rain in RI cases appears to be related to the moistening/humidification of the inner core, and particularly in the upshear quadrants.

The relationship between precipitation asymmetry and TC intensity has also been examined in several aircraft-based observational studies (Rogers et al. 2015, Susca-Lopata et al. 2015, Zawislak et al. 2016, Rogers et al. 2016, Nguyen et al. 2017). In general, the VWS-precipitation relationship is valid for most of the TC cases in these studies. Other factors may also affect the convection and precipitation distribution when the storm undergoes RI under large VWS (e.g., > 10 m s^{-1}), and sometimes even with moderate VWS (e.g., ~ 8 m s^{-1}). For example, asymmetric deep convection in Hurricane Earl (2010) moved from left of the shear to more upshear during the onset of RI (Rogers et al. 2015, Susca-Lopata et al. 2015). During RI,

the precipitation became more axisymmetric when the upper and lower level of the vortex became more vertically aligned.

Hurricane Edouard (2014) was examined by Zawislak et al. (2016) and Rogers et al. (2016). The azimuthal distribution of deep convection was found to be critical to RI. Under VWS, precipitation was first concentrated in the downshear-left quadrant, but then more deep convection developed in the upshear quadrants. When the azimuthal coverage of deep convection increased, especially near the radius of maximum wind, diabatic heating became more symmetric, which has been shown in previous studies to be favorable for rapid intensification.

Nguyen et al. (2017) further discussed several factors that determine precipitation symmetry in sheared TCs such as Hurricanes Bertha and Cristobal (2014). The precipitation asymmetry was greater in Hurricane Cristobal due to convective downdrafts that transported low-entropy air into the boundary layer of the upshear quadrants. In addition, stronger subsidence and advection of mid-level dry air into the upshear quadrants of Hurricane Cristobal contributed to the greater degree of precipitation asymmetry.

6. Improvements in Numerical Models

a. Radar data assimilation

Bao et al. (2017) examined the impact of an improved initial field through assimilating ground-based radar data from mainland China and Taiwan Island to simulate the long-lasting and extreme rainfall caused by Typhoon Morakot (2009). The vortex location and the subsequent track analyzed through radial velocity data assimilation (VDA) were generally consistent with the best track. The initial humidity within the radar detection range and Morakot's northward translation were significantly improved by radar reflectivity data

assimilation (ZDA). As a result, the heavy rainfall on both sides of Taiwan Strait can be replicated with the joint application of VDA and ZDA. In a sensitivity experiment without ZDA, the simulated storm underwent an unrealistic inward contraction after 12-h integration due to an under-estimation of humidity in the global analysis, which leads to an underestimation of rainfall amount and coverage. Without the vortex relocation via VDA, the more moist (drier) initial humidity field with (without) ZDA resulted in a slower (faster) northward translation, which therefore affected the rainfall on both sides of Taiwan Strait. An improvement in the humidity analysis of Morakot was traced to the assimilation of high-value reflectivity (strong convection) observed by the radars on Taiwan Island, and especially at the Kenting radar. Analyses of parcel trajectories and water vapor flux divergence indicated that the improved typhoon circulation achieved through assimilating radar data then resulted in enhanced water vapor fluxes from the environment in the simulation, which subsequently contributed to better predictions of the extreme rainfall on both sides of the Taiwan Strait.

b. Microphysics

The precipitation microphysics also play an important role in predicting extreme events (Bell 2017). Even with the high rainfall accumulations of extreme events, high-resolution mesoscale models can obtain good Quantitative Precipitation Forecast (QPF) skill for even the larger rainfall thresholds (Wang 2015). However, significant sensitivity and uncertainties remain in the parameterization of microphysical processes in numerical weather prediction (NWP) models (Hendricks et al. 2016). These uncertainties are difficult to reduce in large part due to a lack of microphysical observations in TCs. However, recent technological upgrades have great promise in helping to validate and improve parameterizations of warm rain processes. For example, Brown et al. (2016) used polarimetric radar measurements to evaluate several common

microphysics parameterizations in the Weather Research and Forecasting (WRF) model. The Thompson-Eidhammer aerosol-aware bulk and explicit spectral bin microphysical schemes were shown to perform the best. Brown et al. (2017) further improved the Thompson-Eidhammer bulk scheme by changing the number production of rain drops from melting snow, which had no degradation to the short-term intensity simulation. Kalina et al. (2017) applied dual-polarization, scanning radar- and polarimetric radar-based particle identification schemes to analyze the ice water paths (IWP) of small and large particles in Hurricanes Arthur (2014) and Irene (2011). Probability density functions of the small-to-total IWP ratio were found to depend on precipitation type, which can be applied to evaluate microphysics schemes in numerical models.

c. Improved NWP model resolution

Pohl et al. (2016) performed ensemble simulations of TC Ando (31 December 2000–9 January 2001) over the southwest Indian Ocean using the non-hydrostatic WRF ensemble model. Nested domains centered over the island of La Réunion allowed for the simulation of local rainfall amounts associated with TC Ando at very high resolution (680-m grid spacing). The model was nudged toward the ERA-Interim reanalysis during the six days of the TC's life cycle. The length of the nudging was then varied to constrain either the whole life cycle or only parts of it.

As expected, smaller ensemble member dispersion is simulated as the relaxation lasts longer, with more members producing similar cyclone tracks and intensities. The model shows reasonable skill in simulating local rainfall amounts and distributions when the simulated TC approaches La Reunion with a realistic distance and approach direction. Strong lower-level winds associated with the TC circulation ascent over the slopes of the island lead to successful simulations of the extreme daily precipitation amounts (>1200 mm) and even their distribution

over the highest parts of La Reunion. However, smaller-scale features of the rainfall field are less realistic in the simulations. Pohl et al. concluded that the wind speed and direction upstream of the island are the main drivers of such local uncertainties and errors, and these smaller-scale features are an important issue to assess the local impacts of the TC over such a complex terrain.

Wang and Zeng (2018) carried out an investigation of the effect of horizontal resolution on the precipitation of the Super Typhoon Rammasun (2014) using the WRF (V3.4) model with resolutions of 15 km, 9 km, and 3 km. Simulated "Rammasun" rain band shapes and distributions are nearly the same at different horizontal resolutions. When the horizontal grid size is decreased from 15 km to 9 km and then to 3 km, heavy precipitation is simulated to spread in all directions from a concentrated distribution, and especially when the resolution is increased from 9 km to 3 km (**Fig. 7**). The 6-h and 1-h heavy precipitation distributions have more concentrated comma-shapes. Moreover, the simulated water vapor distribution has the same characteristics as the heavy precipitation with a notably enhanced vertical ascending motion and an increased height of the strongest ascent. The precipitation distribution simulated at 3-km resolution is the closest to the observed distribution. However, a noticeable difference exists between the simulated precipitation and the observed distribution. In a sensitivity test omitting the convection parameterization in the model, the precipitation distributions simulated at the 9-km and 3-km resolutions generally have the same features as when the Kain-Fritsch convection parameterization included. However, the simulated precipitation amounts at these two resolutions are smaller than those obtained with the KF scheme included, which provides the best simulation of the Rammasun precipitation.

A very significant heavy rainfall event associated with Typhoon Talas (2011) totaled more than 1000 mm over the Kii Peninsula of Japan with a local maximum of about 1800 mm

due the slow translation speed of Talas. This large rainfall caused many landslides and floods over the Kii Peninsula and led to 98 fatalities. Tsuboki and Sakakibara (2002) and Tsuboki (2008) performed cloud-resolving numerical model simulations (using a model named CReSS) of Typhoon Talas, in which the simulated rainfall intensity was almost the same as the observed rainfall intensity. However, the maximum amount of rainfall was almost one half of the observed total amounts because the stagnation of the typhoon prior to landfall on Japan was not correctly simulated. This simulation is then another example that it is not just the rainrate, but also the duration of that rainfall that is important for predicting the accumulated rain amount, which indicates that the prediction of rainfall period as well as rainfall intensity is important for an accurate forecast of TC rainfall amounts.

Another significant flood event occurred north of Tokyo in association with two typhoons: Typhoons Etau (2015) and Kilo (2015). Whereas Typhoon Etau (2015) moved to the Sea of Japan over the central part of Japan, Typhoon Kilo moved slowly northward to the east of Tokyo over the Pacific. Between these two typhoons, a very intense rainband formed that was almost stationary over the Tokyo area. The CReSS model correctly simulated these two typhoons and showed that a band of large moisture flux extended from the south to the Tokyo area (**Fig. 8**), which is referred to as an atmospheric river. This band extended from the South China Sea to the Tokyo area. Since the atmospheric river brought a large amount of moisture and the large-scale ambient atmospheric field was changing very slowly, the intense rainband remained almost stationary. Consequently, the maximum total rainfall of more than 800 mm occurred to the north of Tokyo.

d. Ensemble quantitative precipitation Forecast

With violent wind and heavy rainfall, the TC is one of the most disastrous weather systems in coastal areas. Hong et. al. (2015) has developed an ensemble typhoon quantitative precipitation forecast (ETQPF) to improve typhoon rainfall prediction. This ETQPF rainfall forecast is obtained by averaging selected ensemble members that meet certain criteria based on the target typhoon track (**Fig. 9**). An online COMET/NOAA module describing the ETQPF (available in traditional Chinese) explains how the typhoon QPF methodology is used by the Taiwan Central Weather Bureau (https://www.meted.ucar.edu/tropical/typhoon_qpf/). Some examples of the rainfall forecasts from the ETQPF model are given in the website link along with the quantitative verifications that illustrate reasonable typhoon rainfall forecasts (**Fig.10**).

In March 2017, three EPSs of the Japan Meteorological Agency (JMA), which were specifically designed for one-week typhoon tracking and one-month forecasts, evolved into a single integrated system called the Global Ensemble Prediction System (GEPS). These typhoon track forecasts and precipitation forecasts based on the GEPS are more accurate compared to the previous systems. Typhoon track forecasts derived from the GEPS, along with forecasts from major centers around the globe, are now available on the RSMC Tokyo's NWP website dedicated to members of the Typhoon Committee.

The JMA disseminates the Very Short-Range Forecast of precipitation (VSRF) up to six hours ahead by blending at an appropriate ratio advection-based extrapolations of radar echoes with precipitation forecasts from high-resolution numerical weather models. The VSRF system has recently undergone some improvements: (i) dynamical optimization of parameters used for adjusting orographic effects on radar echo intensity; (ii) change in blending between predictions based on radar echo advection and numerical models to give more weight to the model forecasts

for earlier forecast hours; and (iii) more appropriate radar echo extrapolation by properly dealing with a rapid change in velocity vectors associated with a precipitation system.

HKO conducted its first feasibility studies on regional mesoscale ensemble prediction after passage of Severe Typhoon Vicente (Hon et al. 2012), which necessitated the issuance of Tropical Cyclone Warning Signal No. 10 in Hong Kong, the highest such signal for the city, at the time. Near real-time trial operation of a 10-km, 20-member, WRF-based mesoscale ensemble prediction system at HKO commenced in late 2013 (Hon 2015) which indicated some benefits for track and rainfall prediction in a number of recent high-impact TC cases (Hon and Hon 2016).

Many national hydrometeorological centers currently apply ensemble products to extend the lead time for TC landfall rainfall forecasts. Since different ensemble systems have different perturbation schemes and methods of TC vortex initialization, their rainfall forecast products may not perform the same in different situations. None of those ensembles always perform the best from case to case, and especially at lead times longer than 2 days. Thus, it was suggested that a calibrated super-ensemble may be a more promising way to obtain skillful rainfall forecast with longer lead times (Qi, personal communication).

e. TC rainfall forecast verifications

Yu et al. (2018) objectively verified the 0-6, 0-24, 24-48, 48-72, and 0-72 h forecast rainfall accumulations for 25 landfalling TCs over China during 2012 – 2015. The sample consisted of 133 operational numerical forecasts from the ACCESS-TC, which is the TC version of the Australian Community Climate and Earth System Simulator. Verifications were performed for the unadjusted forecasts and after applying the Contiguous Rain Area (CRA) method, which helps diagnose the origin of systematic errors via an adjustment of the forecast rain field by displacement, rotation, volume, and pattern. Objective analyses of combined rain gauge and

TRMM satellite observations are used for ground truth. Since the Mean track and intensity forecast errors at 48h for the sample were 180 km and 10 kt, the ACCESS-TC had a quite skillful level of performance.

Mean values of equitable threat score, probability of detection, and false alarm ratio for the 30-mm isohyet for the unadjusted forecasts at 0-6 h (essentially the initialization) are (0.22, 0.56, 0.66) (**Fig. 11**). The skill of the 24-h forecast accumulations is highest (0.36, 0.63, 0.40), and then declines to (0.20, 0.42, 0.60) for the 72-h forecasts. Forecast skill also declines with larger rainfall accumulations.

After application of the CRA method, errors are reduced for very heavy rain amounts by about 15% by accounting for the rainfall patterns, and for the displacement errors. This improvement suggests that rainfall prediction will continue to improve with improved TC track prediction, but more work is needed on initialization and prediction of TC structure. Yu et al. (2018) also presented case studies to illustrate these systematic errors and provide guidance for future efforts on initialization and system development.

7. Forecast Challenges

a. Rainfall Monitoring

The JMA put into operation in August 2014 a high-resolution precipitation nowcasting system (hereafter HRPNS) that was a refinement of the precipitation nowcasting system that had been in operation since 2004. This HRPNS integrated observations from multiple other sources including the X-Band multi-parameter radar information network (XRAIN) deployed by the Ministry of Land Infrastructure, Transport and Tourism (MLIT) into the JMA's Doppler radar network. The HRPNS provides quantitative estimates of precipitation intensity (mm h^{-1}) every 5 minutes at a spatial resolution of 250 m (**Fig. 12**) over a domain that includes the four

main islands and nearly all of the numerous smaller islands of Japan. The implementation of the HRPNS has enhanced the forecaster's capability to monitor fast-changing, intense precipitation systems more accurately as they grow and decay over time. A real-time update of the HRPNS precipitation distribution is publicly available on the JMA's website, and has become one of the most frequently viewed web links during the wet season. Some recent HRPNS improvements have been in quality control aspects, including exploiting satellite images to detect spurious radar echoes and a calibration process relative to in-situ rain gauge data.

In 2017 the JMA started disseminating newly developed hydrological indices that are closely related to flood and inundation risk. These indices indicate varying disaster risk from region to region for a given amount of precipitation due to differences in environmental factors such as orography, land-use conditions, and proximity to a river on a 1-km grid covering Japan (**Fig. 12**). The objective of the indices is to help forecasters and disaster management officers to understand the areas and magnitudes of the elevated risk.

Nowcasting plays an important role in forecasting and warning of heavy rainfall due to TC in megacities and metropolitan area like Hong Kong. HKO continues to develop and operate the "SWIRLS nowcasting system" for quantitative precipitation estimates and forecasts as well as predictions of lightning (Chan and Woo 2018) and other severe weathers. Starting from 2015, a community version of SWIRLS was provided to interested meteorological services (Wong et al. 2016). While the operational SWIRLS employs variational optical flow (Woo and Wong 2017), the potential use of deep learning were explored with thedevelopments of recurrent neural networks based on convolutional Long Short Term Memory (LSTM) (Shi et al. 2015) and trajectory Gated Recurrent Unit (GRU) (Shi et al. 2017a). A technique to retrieve

reflectivity from Himawari-8 was developed and verified to achieve useful results (Woo et al. 2017), which could supplement radar observations and provide valuable information over oceans and seas.

b. Similar TC landfall locations, but different impacts

Super Typhoons Nepartak and Meranti made landfall in July and September 2016, at almost the same location, south of Fujian province in China, and then move northward along the same track to Taihu Lake Basin (hereafter as TLB). Although their tracks over land were the same, rainfall amounts and distributions relative to these TCs and their remnants were all different (**Fig. 13**). Shi et al. (2017b) explained the different rainfall distributions in terms of the different intensities and structures for the two TYs, and the different synoptic situations during/after their landfalls.

Before making landfall on mainland China, Nepartak had passed over southern Taiwan, and then stagnated over the Taiwan Strait for nearly 24 h. Thus, Nepartak made landfall on mainland China as a Severe Tropical Storm (STS, 25 m s^{-1}) without a well-developed innercore (**Figs. 14a and c**), and the rainfall was small and concentrated in the landfall area. By contrast, Meranti made landfall with an intensity of Strong Typhoon (STY, 50 m s^{-1}). After its landfall, Meranti maintained a TC-like vortex structure for nearly 24 h after landfall with heavy rainfall at the landfalling location area and along its northward track (**Figs. 14b and d**).

Since Nepartak landed in mid-summer, its northward track was along the western edge of the sub-tropical high with a midlatitude trough approaching from north China (not shown). During the summer, westerly troughs are concentrated in the upper levels (higher than 600 hPa), and the upper level cold air mainly causes localized thunderstorms rather than widespread heavy rainfall. By contrast, Meranti occurred in September when the westerly troughs extend to lower

levels (below 850 hPa). The interaction of such a cold trough with Meranti's remnant lead to frontogenesis (not shown), and widespread heavy rainfall occurred at TLB, which is 600-800 km from Meranti's landfall location.

Both the ECMWF-IFS and the NCEP-GFS had fairly good guidance for Meranti's precipitation even at leadtimes longer than 2 days. But for Nepartak's rainfall forecast, models' guidance was not so satisfying. At lead time longer than 2 days, global models, including their ensemble ones, present guidance of obvious heavy rainfall at TLB which misled forecasters at that time (not shown). Within 2 days, global models' rainfall guidance was fairly successful, especially at TLB. All models did not forecast heavy rainfall at TLB, which agreed well with the observation (not shown). The fundamental reasons why all models forecast heavy rainfall at TLB by Nepartak's remnant for lead time longer than 2 days are not easy to understand. But it seems related to model's unrealistic deepening of Nepartak's remnant at TLB (**Figs. 15a, c**). In fact, Nepartak keeps weakening after its landing and its remnant does not show a re-developing process when it passes over TLB (Fig. 14a). Within 2 days, models begin to forecast a weakening remnant at TLB which bring up with a better precipitation forecast also (**Figs. 15b and d**).

c. Anomalous typhoon activity and landfall in August 2016

After TC activity was exceptionally suppressed early in the 2017 northwest Pacific basin, seven typhoons (tropical storm intensity or higher) formed in August 2016. Four TCs (Chanthu, Mindulle, Lionrock, and Kompasu), made landfall in rapid succession on the Japanese mainland, which ties the record for the largest number of typhoon landfalls over the country in a single month. This pattern of typhoon activity was also unusual in that all four typhoons had northward tracks and eventually hit the Pacific coast of northern Japan (**Fig. 16 upper**), which experiences

even a single typhoon landfall. Primarily due to rainfall from these four typhoons, the regional average monthly precipitation at 231% of normal on the Pacific side of northern Japan for August was the highest on record since 1946 (**Fig.16 lower**). More than 20 fatalities and substantial damages to houses, infrastructure, and agriculture were reported due to a recurrence of heavy precipitation events that led to river overflows and flooding.

The active genesis of typhoons in August 2017 was associated with large cyclonic circulation anomalies in the lower troposphere throughout much of the tropical western North Pacific. The pronounced cyclonic circulation, which persisted through the month, resembled the well-known Matsuno-Gill response to an anomalous heating source and may be linked to continuous active convection to the southeast (**Fig. 17**). The intensified convection in turn was sustained by repeated intrusions of high potential vorticity air associated with the persistent trough over the mid-latitude Pacific. In addition, the northwestern Pacific subtropical high (NWPSH) was displaced far eastward of its normal position in August 2016, in association with a persistent wave train pattern in the upper troposphere extending from Eurasia to the mid-Pacific. The absence of the NWPSH over and to the immediate east of Japan made it possible for the typhoons to have tracks due northward just east of Japan to wreak havoc in the northern part of the country.

8. Concluding Remarks

Progress in research and forecast techniques related to TC rainfall since the last IWTCLP in 2014 has been summarized in this article. One advance has been in the understanding of the contribution of TCs to global rainfall, including extreme rainfall, and its regional trends. There have been field experiment studies on TC rainband dynamics, including observations of microphysical processes in TC rainbands, and with possible enhanced rainfall due to topographic

effects. The individual case studies and climatological studies have increased understanding of TC rainfall patterns in different intensification stages, including during the RI phrase. These rainfall patterns associated with convective and stratiform rain may be useful in improving intensity forecasts. Environmental interactions may modify the TC rainfall pattern substantially and generate remote rainfall events, which is one of the challenges in forecasting rainfall. Environmental VWS has been a major focus for studies in the last few years. Analyses of TC cases under strong and weak environmental VWS have revealed the degree of modulation of rainfall asymmetry by such an environmental factor. When environmental VWS is weak, factors such as internal rainband dynamics, mesoscale processes within TCs, and land-sea contrasts may have larger roles in TC rainfall changes.

Many advances have been made in TC rainfall simulations by NWP models. These advances include improved resolution of models, better representation of microphysical processes based on field experiment observations, and improved data assimilation techniques of radar and other remote-sensing data. Ensemble forecasting systems especially designed for TC rainfall have been developed that show promising forecast skill over previous ensemble systems. These systems adopt a case selection approach that better captures the climatological rainfall characteristics of TC cases with similar locations and track types. Nevertheless, advanced verification techniques are needed that reveal NWP models' inadequacies and weaknesses. One recent model verification study clearly showed that simulating the correct TC structure is an important factor in improving the rainfall distribution in model forecasts.

Ground-based radars, airborne radars and satellite observations of TC rainfall have been improved. These platforms expose different aspects of the rainfall processes within TCs, and it is important for forecasters to understand the processes behind these observations and appropriately

interpret them. Physical interpretations of those observations are also valuable for developing conceptual models of TC rainfall, and NWP model evaluations. Some operational centers have generated high-fidelity nowcasting systems that integrate various modes of rainfall observations, which help forecasters' understanding of rainfall pattern and their interpretation process. It is suggested that all operational centers investigate the most appropriate nowcasting systems for their applications and make these systems available to forecasters. After discussion among the participants at the IWTCLP-IV, several recommendations have been made to the research and operational community, and the WMO based on our review of the TC rainfall focus area. These recommendations will be made available at the WMO website.

Although this article focuses on the weather forecasting timescale, other studies have projected future TC activity and rainfall patterns under climate and environmental change. Changes in TC rainfall patterns are most due to changes in TC tracks and intensity (e.g., Tsuboki et al. 2015). If realized, future rainfall distributions on local to regional scales would be different from previous climatology, and continuous monitoring on such time and space scales is essential for future improvements in TC rainfall forecasting.

Acknowledgments. The first three authors (KC, ZY and RLE) would like to thank all the working group members (as coauthors of this article) who have contributed to the rapporteur report on the TC rainfall focus area of the IWTLCP-IV. Their orders in co-authorship are according to their last names and not the degree of contribution. The discussion by all the participants of the workshop has helped in the selection of content for this article. The authors would also like to thank Mr. W. K. Wong, Mr. W. C. Woo and Mr. K. K. Hon of the Hong Kong Observatory for their valuable comments and inputs to the manuscript.

References

Bagtasa, G., 2017: Contribution of tropical cyclones to rainfall in the Philippines. *J. Climate*, **30**, 3621–3633.

Bao, X., N. E. Davidson, H. Yu, M. C. N. Hankinson, Z. Sun, L. J. Rikus, J. Liu, Z. Yu, and D. Wu, 2015: Diagnostics for an extreme rain event near Shanghai during the landfall of Typhoon Fitow (2013*). Mon. Wea. Rev*., **143**, 3377–3405.

Bao, X., D. Wu and co-authors, 2017: Improving extreme rainfall forecast of Typhoon Morakot (2009) by assimilating radar data from Taiwan and mainland China. *J. Meteor. Res.*, **31**, 747–766.

Bell, M. M., 2017: Extreme precipitation from tropical cyclones. Invited Review at the *Sixth International Workshop on Monsoons* (IWM-VI), World Meteorological Organization, 13-17 November, Singapore.

Breña-Naranjo, J. A., A. Pedrozo-Acuña, O. Pozos-Estrada, S. A.Jiménez-López, and M. R. López-López, 2015: The contribution of tropical cyclones to rainfall in Mexico. *Phys. Chem. Earth*, **83–84**, 111–122.

Brown, B. R., M. M. Bell, and A. Frambach, 2016: Validation of simulated hurricane drop size distributions using polarimetric radar. *Geophys. Res. Lett*., **43**, doi:10.1002 /2015GL067278.

Brown, B. R., M. M. Bell, and G. Thompson, 2017: Improvements to the snow melting process in a partially double moment microphysics parameterization, *J. Adv. Model. Sys*., **9**, 1150–1166.

Chan, N. H., and W. C. Woo, 2018: Location specific lightning nowcast service, *The 32th Guangdong-Hong Kong-Macau Seminar on Meteorological Technology*, Macau, 8-9 January 2018

Chen, F., and Y. Fu, 2015: Contribution of tropical cyclone rainfall at categories to total precipitation over the western North Pacific from 1998 to 2007. *Sci. China Earth Sci.*, **58**, 2015–2025.

Chen, S. S., J. A. Knaff, and F. D. Marks, 2006: Effects of vertical wind shear and storm motion on tropical rainfall asymmetries deduced from TRMM. *Mon. Wea. Rev.*, **134**, 3190–3208.

Corbosiero, K.L. and J. Molinari, 2003: The relationship between storm motion, vertical wind shear, and convective asymmetries in tropical cyclones. *J. Atmos. Sci*., **60**, 366–376.

DeHart, J.C. and R. A. Houze, 2017: Orographic modification of precipitation processes in Hurricane Karl (2010). *Mon. Wea. Rev*., **145**, 4171–4186.

DeMaria, M., C. R. Sampson, J. A. Knaff, and K. D. Musgrave, 2014: Is tropical cyclone intensity guidance improving? *Bull. Amer. Meteor. Soc*., **95**, 387–398.

Deng, D., N. E. Davidson, L. Hu, K. J. Tory, M. C. N. Hankinson, and S. Gao, 2017: Potential vorticity perspective of vortex structure changes of Tropical Cyclone Bilis (2006) during a heavy rain event following landfall. *Mon. Wea. Rev*., **145**, 1875–1895.

Galarneau, T. J., 2015: Influence of a predecessor rain event on the track of Tropical Cyclone Isaac (2012). *Mon. Wea. Rev*., **143**, 3354–3376.

Guo, L., N. P. Klingaman, P. L. Vidale, A. G. Turner, and Marie-Estelle Demory, 2017: Contribution of tropical cyclones to atmospheric moisture transport and rainfall over East Asia. *J. Climate*, **30**, 3853–3865.

Hendricks, E. A., Y. Jin, J. R. Moskaitis, J. D. Doyle, M. S. Peng, C.-C. Wu, and H.-C. Kuo, 2016: Numerical simulations of Typhoon Morakot (2009) using a multiply nested tropical cyclone prediction model. *Weather and Forecasting*, **31**, 627–645.

Hon, K. K., M. K. Or, and W. K. Wong, 2012: Numerical simulation studies on Severe Typhoon Vicente. The Hong Kong Meteorological Society Bulletin, **22,** 3-30.

Hon, K. K., 2015: First experiments on mesoscale ensemble prediction over the South China coastal areas. The 2930th Guangdong-Hong Kong-Macau Seminar on Meteorological Technology, Macau, 20-22 January 2015.

Hon, W. Y., and K. K. Hon, 2016: First experiments on mesoscale probabilistic tropical cyclone prediction over the South China coastal areas. The 30th Guangdong-Hong Kong-Macau Seminar on Meteorological Technology, Guangzhou, 20-22 April 2016.

Hong, J.-S., C.-T. Fong, L.-F. Hsiao, Y.-C. Yu, and C.-Y. Tzeng, 2015: Ensemble typhoon quantitative precipitation forecasts model in Taiwan. *Weather and Forecasting*, **30**, 217–237.

Houze, R. A., Jr., 2012: Orographic effects on precipitating clouds. *Rev. Geophys.*, **50**, RG1001, doi:10.1029/2011RG000365.

Jiang, H., 2012: The relationship between tropical cyclone intensity change and the strength of inner-core convection. *Mon. Wea. Rev*., **140**, 1164–1176.

Jiang, H., and E. M. Ramirez, 2013: Necessary conditions for tropical cyclone rapid intensification as derived from 11 years of TRMM data. *J. Climate*, **26**, 6459–6470.

Kalina E. A., S. Y. Matrosov, J. J. Cione, F. D. Marks, J. Vivekanandan, R. A. Black, J. C. Hubbert, M. M. Bell, D. E. Kingsmill, and A. B. White, 2017: The ice water paths of small and large ice species in Hurricanes Arthur (2014) and Irene (2011). *J. Appl. Meteor. Clim*., **56**, 1383–1404.

Khouakhi, A., G. Villarini, and G. A. Vecchi, 2017: Contribution of tropical cyclones to rainfall at the global scale, *J. Climate*, **30**, 359–372.

Li, C. Y. R., W. Zhou, and T. Cheung Lee, 2015: Climatological characteristics and observed trends of tropical cyclone–induced rainfall and their Influences on long-term rainfall variations in Hong Kong. *Mon. Wea. Rev*., **143**, 2192–2206.

Marchok, T. *et al.*, 2014: Summary of recent research related to rainfall, *the Eighth International Workshop on Tropical Cyclones cum the Third International Workshop on Tropical Cyclone Landfall Processes*, 2 – 10 December 2014, Jeju, Korea

Ng, B., K. Walsh, and S. Lavender, 2015: The contribution of tropical cyclones to rainfall in northwest Australia. *Int. J. Climatol.*, **35**, 2689–2697

Nguyen, L. T., R. F. Rogers, and P. D. Reasor, 2017: Thermodynamic and kinematic influences on precipitation symmetry in sheared tropical cyclones: Bertha and Cristobal (2014). *Mon. Wea. Rev.*, **135**, 4423–4446.

Pohl, B., B. Morel, C. Barthe, and O. Bousquet, 2016: Regionalizing rainfall at very high resolution over La Réunion Island: A case study for Tropical Cyclone Ando. *Mon. Wea. Rev.*, **144**, 4081–4099.

Prat, O. P., and B. R. Nelson, 2016: On the link between tropical cyclones and daily rainfall extremes derived from global satellite observations. *J. Climate*, **29**, 6127–6135.

Reasor, P.D., R.F. Rogers, and S. Lorsolo, 2013: Environmental flow impacts on tropical cyclone structure diagnosed from airborne Doppler radar composites. *Mon. Wea. Rev*., **141**, 2949–2969.

Rogers, R. F., R. D. Reasor, and J. A. Zhang, 2015: Multiscale structure and evolution of Hurricane Earl (2010) during rapid intensification. *Mon. Wea. Rev.*, **143**, 536–562.

Rogers, R. F., J. A. Zhang, J. Zawislak, H. Jiang, G. R. Alvey III, E. J. Zipser, and S. N. Stevenson, 2016: Observations of the structure and evolution of hurricane Edouard (2014) during intensity change. Part II: Kinematic structure and the distribution of deep convection. *Mon. Wea. Rev.*, **144**, 3355–3376.

Shi, X., Z. Chen, H. Wang, D. Y. Yeung, W. K. Wong, and W. C. Woo, 2015: Convolutional LSTM network: A machine learning approach for precipitation nowcasting. In *Advances in neural information processing systems*, 802–810.

Shi, X., Z. Gao, L. Lausen, H. Wang, D. Y. Yeung, W. K. Wong, and W. C. Woo, 2017a: Deep Learning for Precipitation Nowcasting: A Benchmark and A New Model. *arXiv preprint arXiv:1706.03458*.

Shi, C., J. Wu, and L. Qi, 2017b: Analysis on precipitation difference of two typhoons with similar tracks. *J. Marine Meteor.*, **37**, 36–45, DOI:10.19513 (in Chinese).

Susca-Lopata, G., J. Zawislak, E. J. Zipser, and R. F. Rogers, 2015: The role of observed environmental conditions and precipitation evolution in the rapid intensification of Hurricane Earl (2010). *Mon. Wea. Rev.*, **143**, 2207–2223.

Tang, X., W.-C. Lee, and M. Bell, 2014: A squall-line-like principal rainband in Typhoon Hagupit (2008) observed by airborne doppler radar. *J. Atmos. Sci.*, **71**, 2733–2746.

Tao, C., and H. Jiang, 2015: Distributions of shallow to very deep precipitation-convection in rapidly intensifying tropical cyclones. *J. Climate*, **28**, 8791–8824.

Tao, C., H. Jiang, and J. Zawislak 2017: The relative importance of stratiform and convective rainfall in rapidly intensifying tropical cyclones. *Mon. Wea. Rev*., **145**, 795–809.

Tsuboki, K. and A. Sakakibara, 2002: Large scale parallel computing of Cloud Resolving Storm Simulator. *High Performance Computing, Springer*, H. P. Zima et al. Eds, 243–259.

Tsuboki, K., 2008: High-resolution simulations of high-impact weather systems using the cloud-resolving model on the Earth Simulator. *High Resolution Numerical Modeling of the Atmosphere and Ocean, Springer, New York, Kevin Hamilton and Wataru Ohfuchi (Eds)*, 141-156.

Tsuboki, K., M. K. Yoshioka, T. Shinoda, M. Kato, S. Kanada, and A. Kitoh, 2015: Future increase of super-typhoon intensity associated with climate change. *Geophys. Res. Lett.*, **42**, 646-652.

Villarini, G., and R. F. Denniston, 2016: Contribution of tropical cyclones to extreme rainfall in Australia. *Int. J. Climatol.*, **36**, 1019–1025.

Wang, C., and Z. Zeng, 2018: The effect of model horizontal resolution on the precipitation of "Rammasun". *Journal of Tropical Meteorology* (in press).

Wang, C.-C., 2015: The more rain, the better the model performs—The dependency of quantitative precipitation forecast skill on rainfall amount for typhoons in Taiwan. *Mon. Wea. Rev*., **143**, 1723–1748.

Wang C.-C., H.-C. Kuo, R. H. Johnson, C.-Y. Lee, S.-Y. Huang, and Y.-H. Chen, 2015: A numerical study of convection in rainbands of Typhoon Morakot (2009) with extreme rainfall: roles of pressure perturbations with low-level wind maxima. *Atmos. Chem. Phys*., **15**, 11097–11115.

Wong, W. K., T. L. Cheng, and W. C. Woo, 2016: Community version of SWIRLS nowcasting system, *WMO WWRP 4th International Symposium on Nowcasting and Very-short-range Forecast 2016 (WSN16)*, 25 – 29 July 2016, Hong Kong, China.

Woo, W. C., *et al.*, 2014: Forecasting challenges related to rainfall, *the Eighth International Workshop on Tropical Cyclones cum the Third International Workshop on Tropical Cyclone Landfall Processes*, 2 – 10 December 2014, Jeju, Korea.

Woo, W. C., Y. Y. Ip, W. K. Wong, and N. H. Chan, 2017: Development of Satellite Reflectivity Retrieval Technique for Tropical Cyclone Rainfall Nowcasting, *Fourth International Workshop on Tropical Cyclones Landfall Processes (IWTCLP-4)*, 5 -7 December 2017, Macau, China.

Woo, W. C. and W. K. Wong, 2017: Operational application of optical flow techniques to radar-based rainfall nowcasting. *Atmosphere*, **8**, 48.

Yu, H., 2014: Rainfall (Topic 8), Chair Report of the *Third International Workshop on Tropical Cyclone Landfall Processes* (IWTCLP-III), World Meteorological Organization, 8-10 December, Jeju, Republic of Korea.

Yu, Z., Y. Wang and H. Xu, 2015: Observed rainfall asymmetry in tropical cyclones making landfall over China. *J. Appl. Meteor. Climatol.*, **54**, 117–136.

Yu, Z., Y. Wang, H. Xu, N. E. Davidson, Y. Chen, Y. Chen, and H. Yu, 2017: On the relationship between intensity and rainfall distribution in tropical cyclones making landfall over China. *J. Appl. Meteor. Climatol.*, **56**, 2883–2901.

Yu, Z., H. Y. Chen, B. Ebert, N. E. Davidson, Y. Xiao, H. Yu. and Y. Duan, 2018: Benchmark rainfall verification of ACCESS-TC operational landfall forecasts over China, *Meteorological Applications*. (submitted).

Zagrodnik, J. P., and H. Jiang, 2014: Rainfall, convection, and latent heating distributions in rapidly intensifying tropical cyclones. *J. Atmos. Sci*., **71**, 2789–2809.

Zawislak, J., H. Jiang, G. R. Alvey III, E. J. Zipser, R. F. Rogers, J. A. Zhang, and S. N. Stevenson, 2016: Observations of the structure and evolution of hurricane Edouard (2014) during intensity change. Part I: Relationship between the thermodynamic structure and precipitation. *Mon. Wea. Rev.*, **144**, 3333–3354.

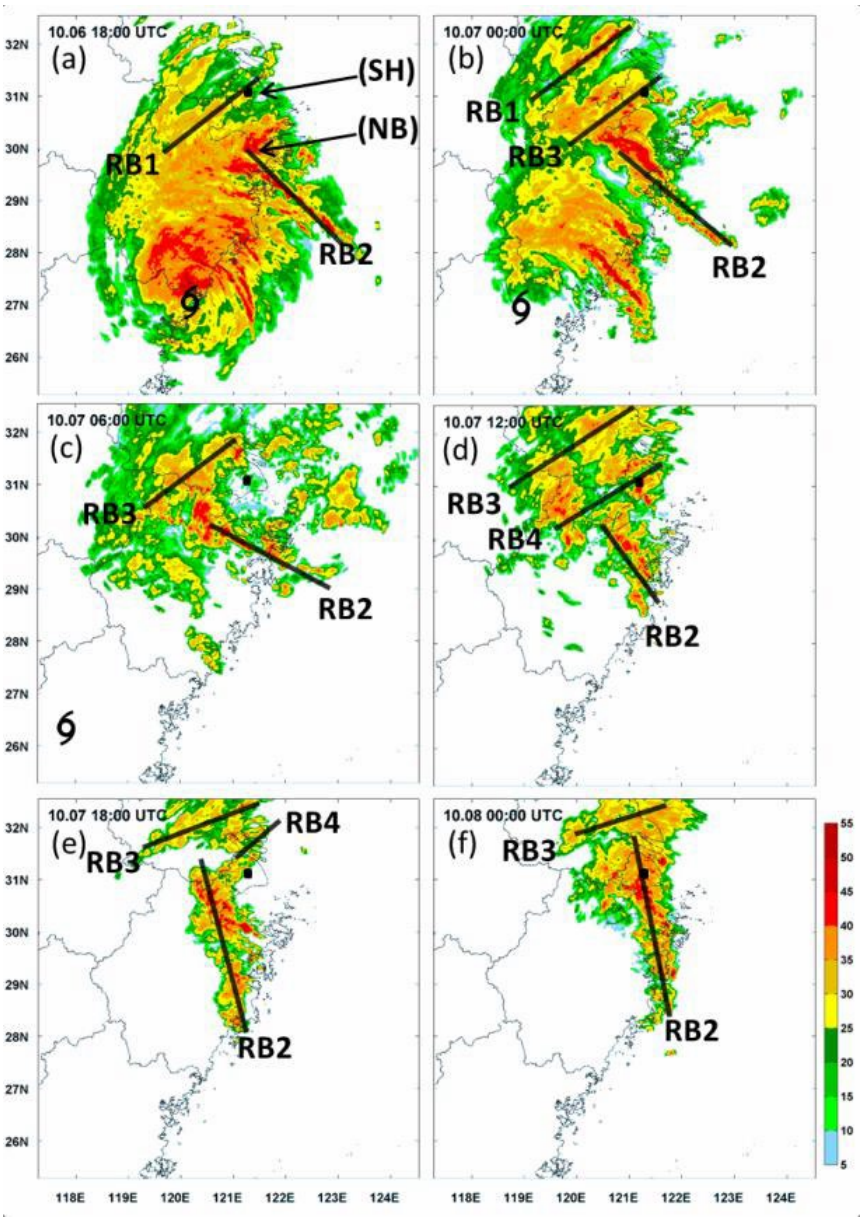

Fig. 1 Six-hourly radar reflectivity of Typhoon Fitow (2013) (Bao et al. 2015).

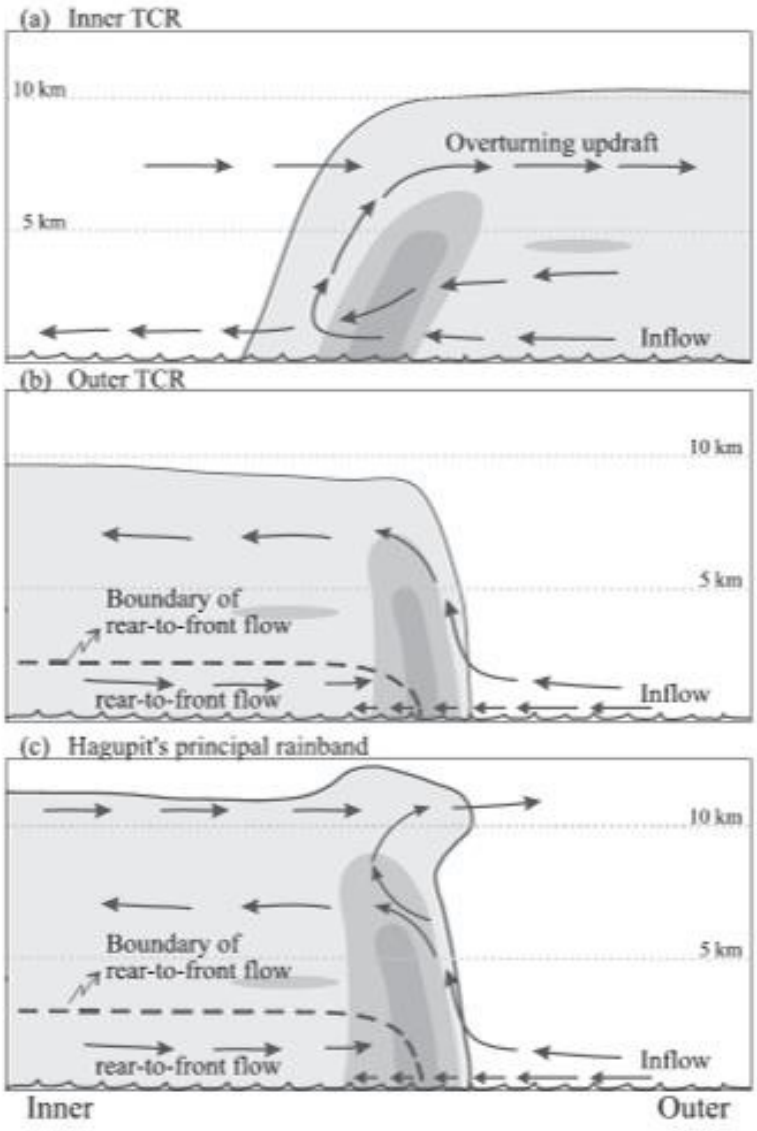

Fig. 2 A comparison of schematics [based on Yu and Tsai (2013)] of vertical structure of different rainbands. Gray colors from light to dark indicate the edges of 10, 25, and 35dBZ, respectively. (a) Inner rainbands and previously documented principal rainbands. (b) Outer rainbands. (c) Hagupit's principal rainband (Tang et al 2014).

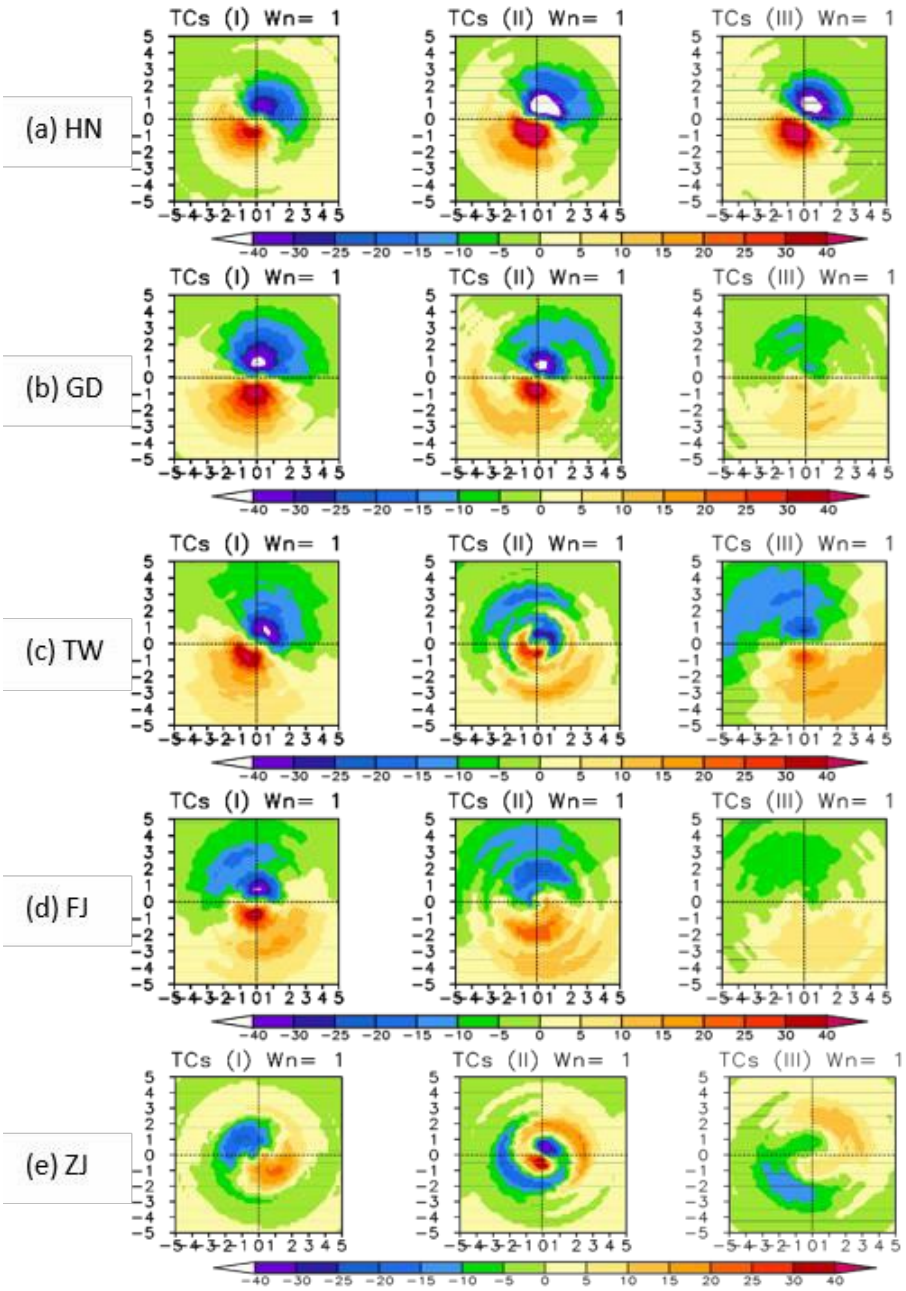

Fig. 3 The wavenumber-one rainfall asymmetry (unit: mm) as a function of distance from the storm center for TCs making landfall at different regions: (a) Hainan, (b) Guangdong, (c) Taiwan, (d) Fujian, and (e) Zhejiang in three stages. X and Y axes are distance (degree) from the TC center (origins). Stage (I) is 24-h prior to landfall, stage (II) is at the time of landfall, and stage (III) is 24-h after landfall. The color scale indicates the amplitude of the asymmetry relative to the distance from the TC center (Yu et al. 2015).

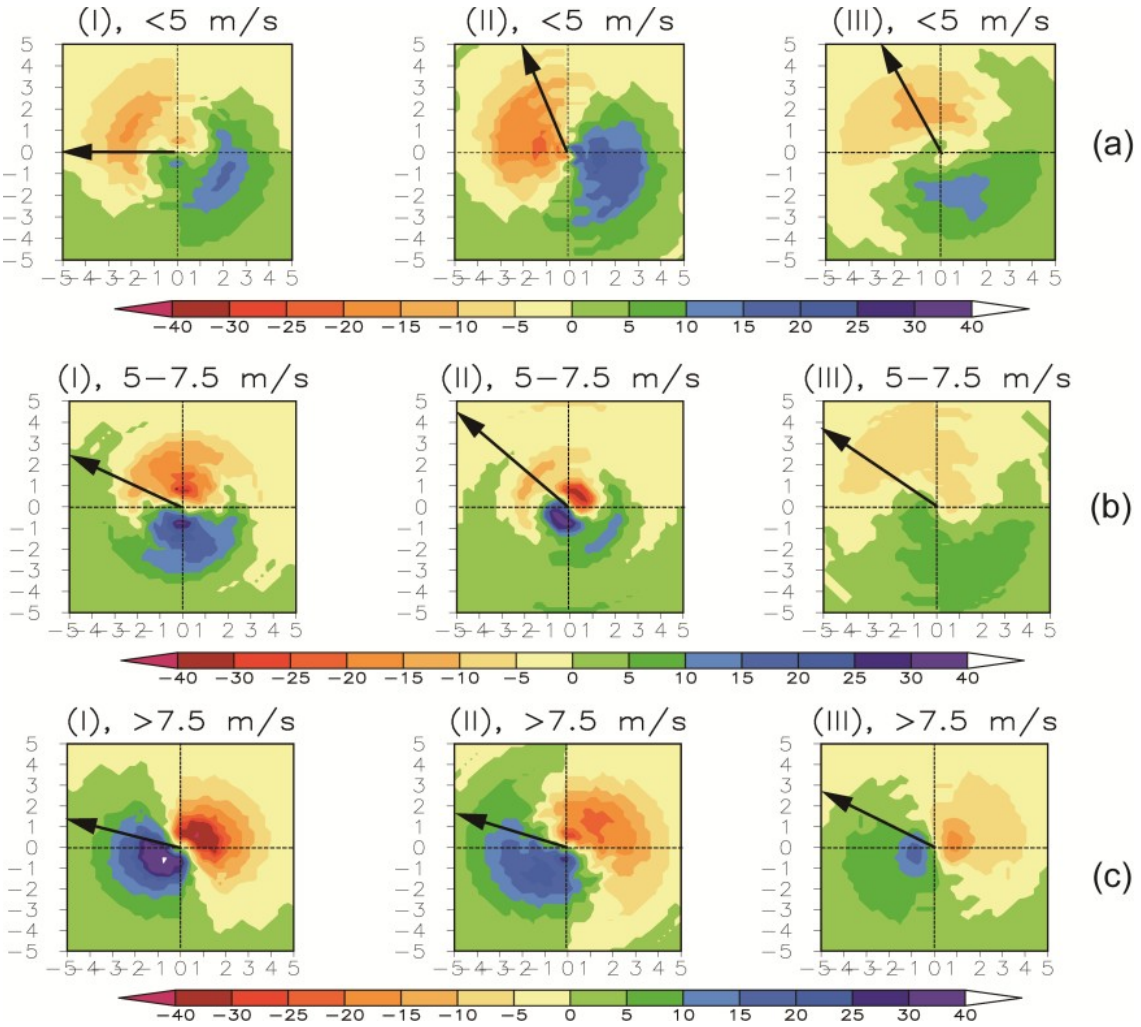

Fig. 4 The wavenumber-1 rainfall asymmetry (shaded, mm) relative to the coastlines for TCs with different VWS magnitudes: (a) <5 m s^{-1}, (b) 5-7.5 m s^{-1}, and (c) > 7.5 m s^{-1}. The solid arrows denote the averaged VWS vectors. The coastline is aligned with the positive X axis to the right (shown by the black solid lines) (Yu et al. 2017).

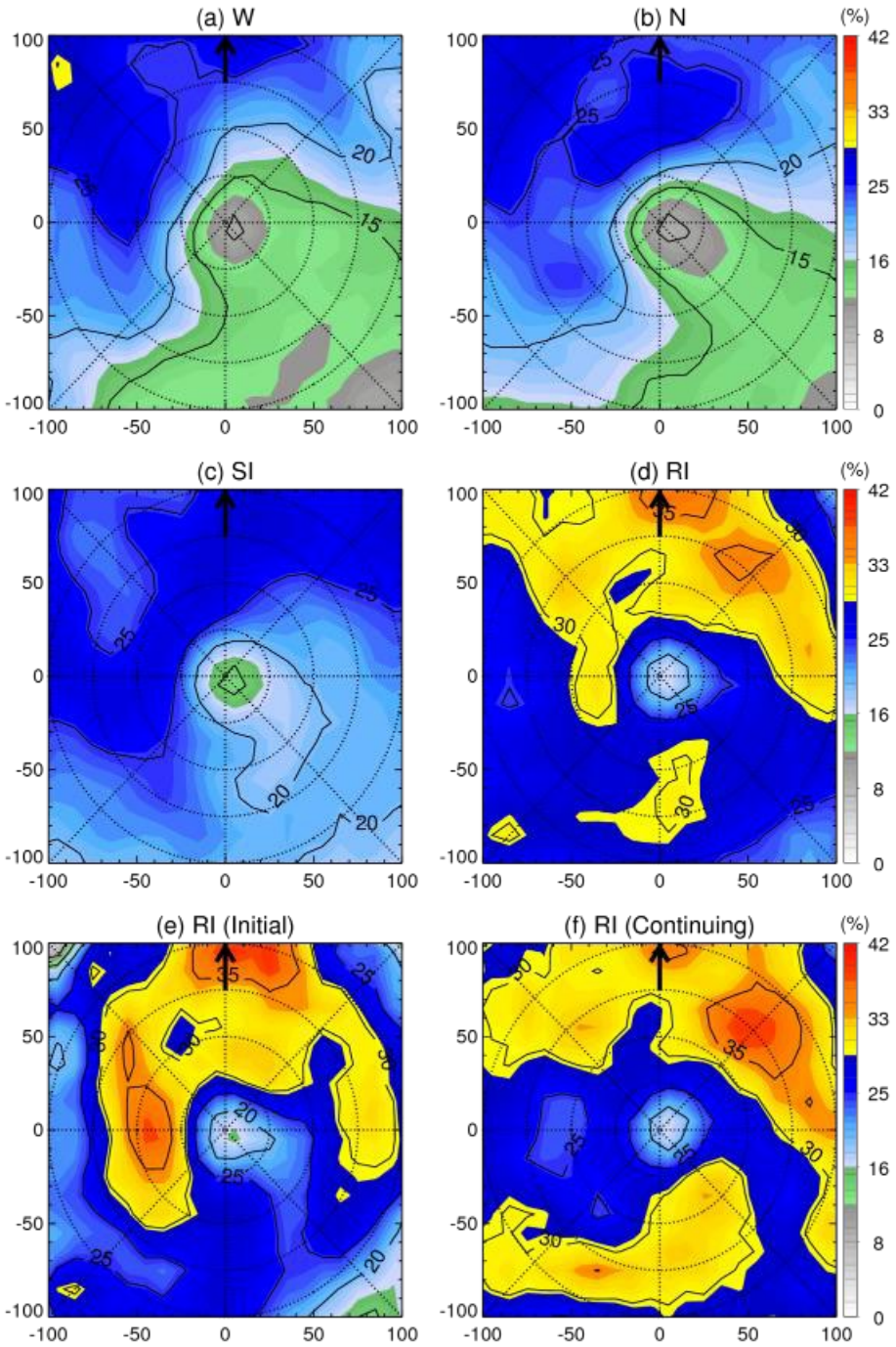

Fig. 5 Composite shear-relative distribution of the percent occurrence of shallow precipitation for (a) Weakening (W), (b) Netural (N), (c) Slowly Intensifying (SI), (d) RI, (e) RI initial, and (f) RI continuing. The black arrow represents the orientation of the vertical wind shear vector. The 25, 50, 75, and 100 km radii are shown as dotted rings (Tao and Jiang 2015).

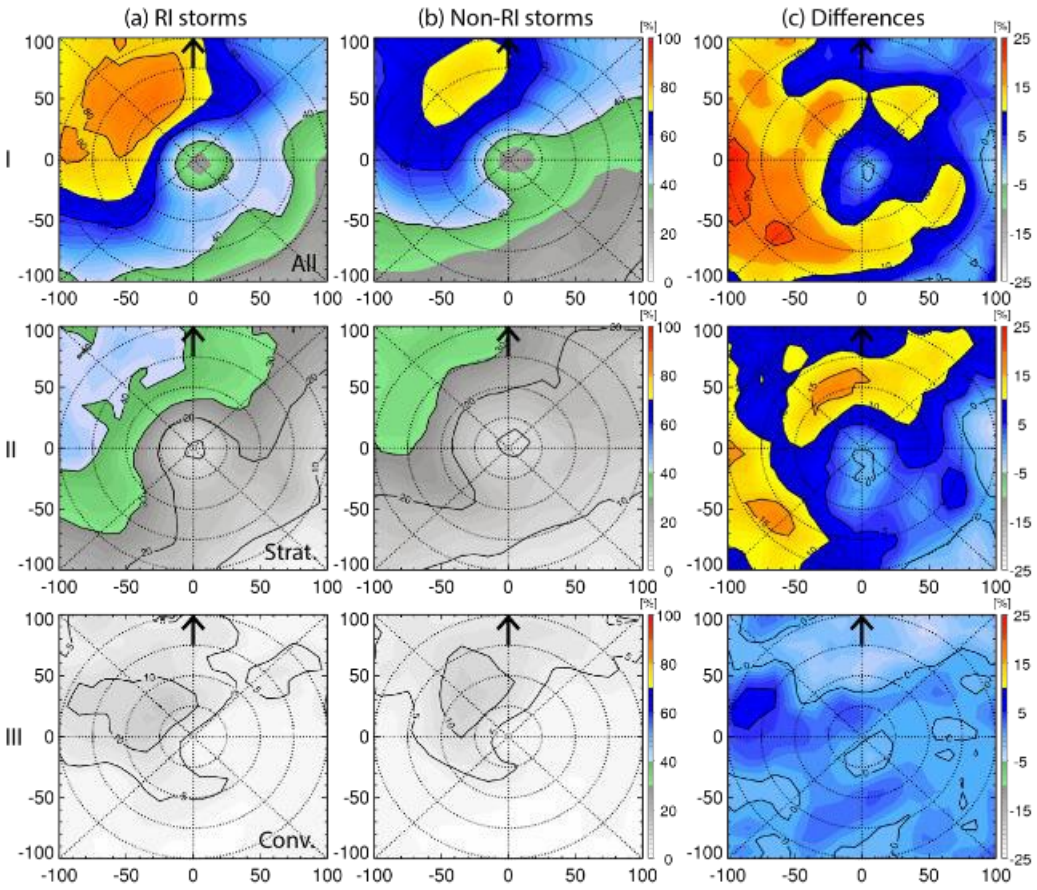

Fig. 6 The Composite shear-relative distributions of the rainfall coverage from (I) all precipitation, (II) stratiform precipitation, and (III) convective precipitation. From left to right: (a) SI cases from RI storms (i.e., 0-12 h before RI onset), (b) SI cases from non-RI storms, and (c) difference between SI cases from RI and from non-RI storms. Dotted range rings represent the 25-, 50-, 75-, and 100-km radii. The black arrow represents the vertical wind shear direction (Tao et al. 2017).

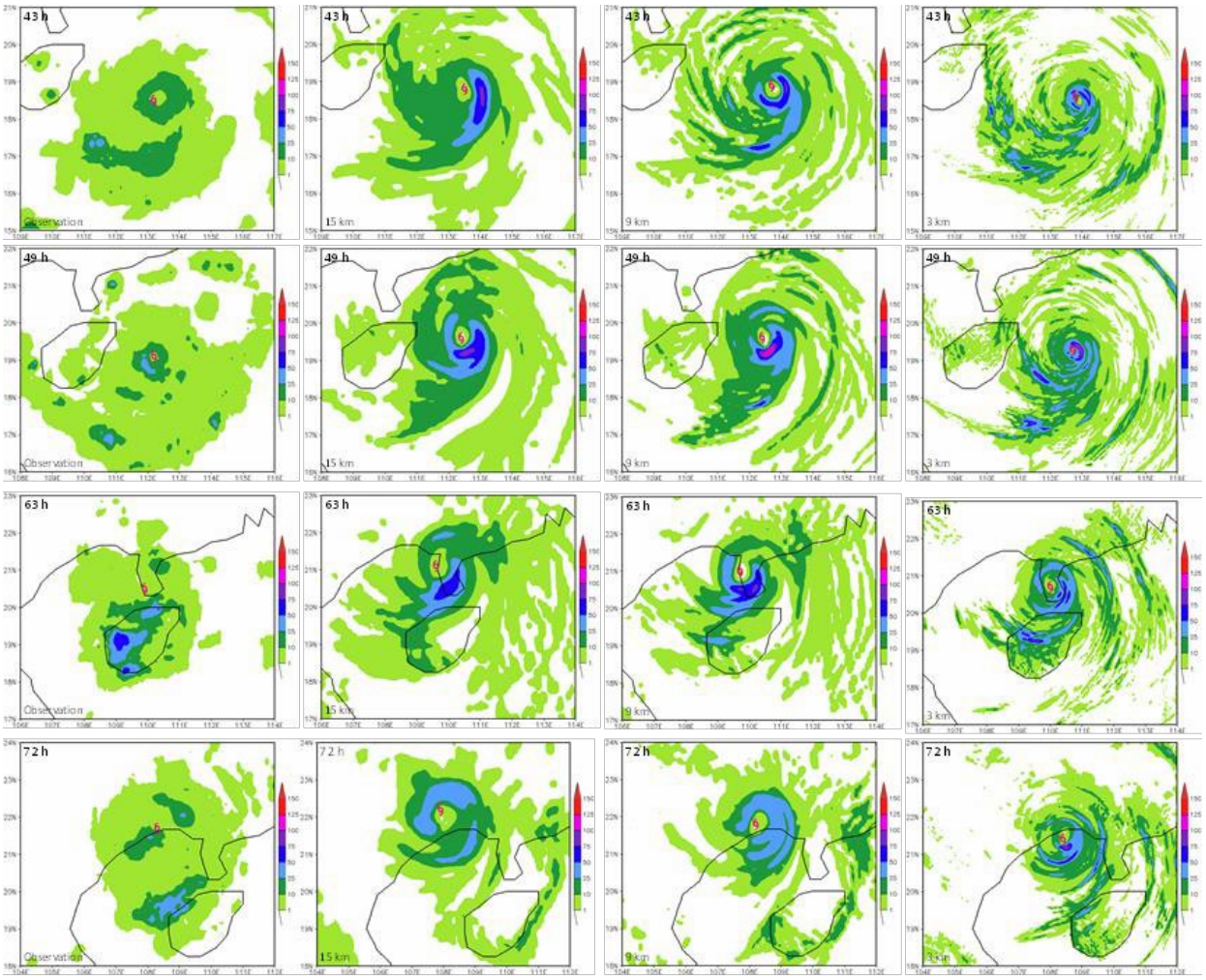

Fig. 7 The observed (column 1) and simulated (with three horizontal resolutions) (column 2-4) 1-h precipitation of Typhon Rammasun (unit: mm; column 2: 15 km, column 3: 9 km, column 4: 3 km; row 1: 43 h, row 2: 49 h, row 3: 63 h, row 4: 72 h). The typhoon symbol shows the position of Rammasun's center (Wang and Zeng 2018).

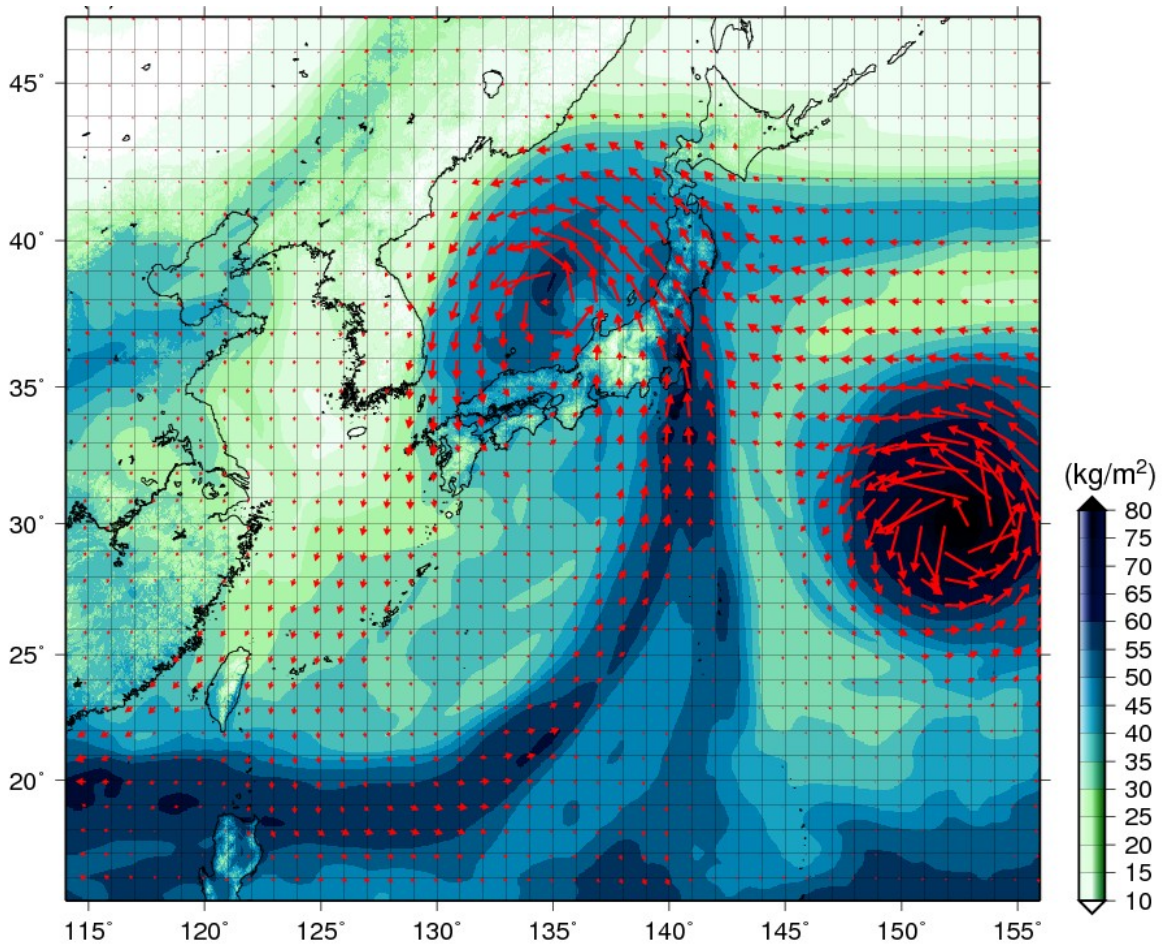

Fig. 8 Vertically integrated water vapor amount (shadings; kg m^{-2}) at 18 JST September 9, 2015, obtained from the simulation experiment using CReSS. The arrows are vertically averaged moisture flux (Tsuboki personal communication).

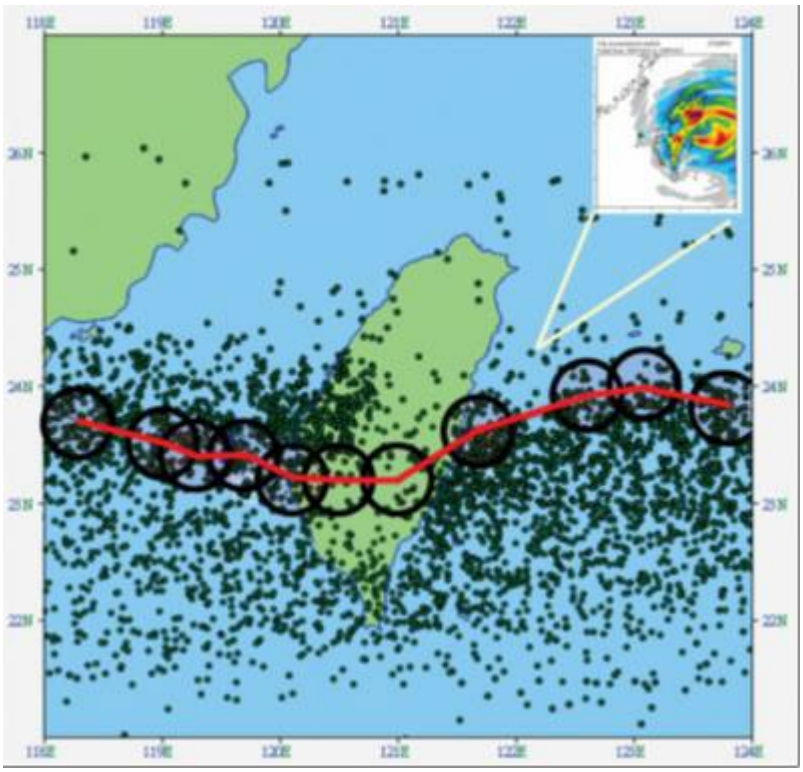

Fig. 9 The predicted typhoon location distribution (black dots) in 3-h intervals from the EPS. Each predicted typhoon location is associated with a 3-h accumulated model QPF; an example is shown in the top-right corner. The red line and black circle are the given typhoon track with 3-h intervals and a radius of 30km centered at each typhoon position, respectively (Hong et al. 2015).

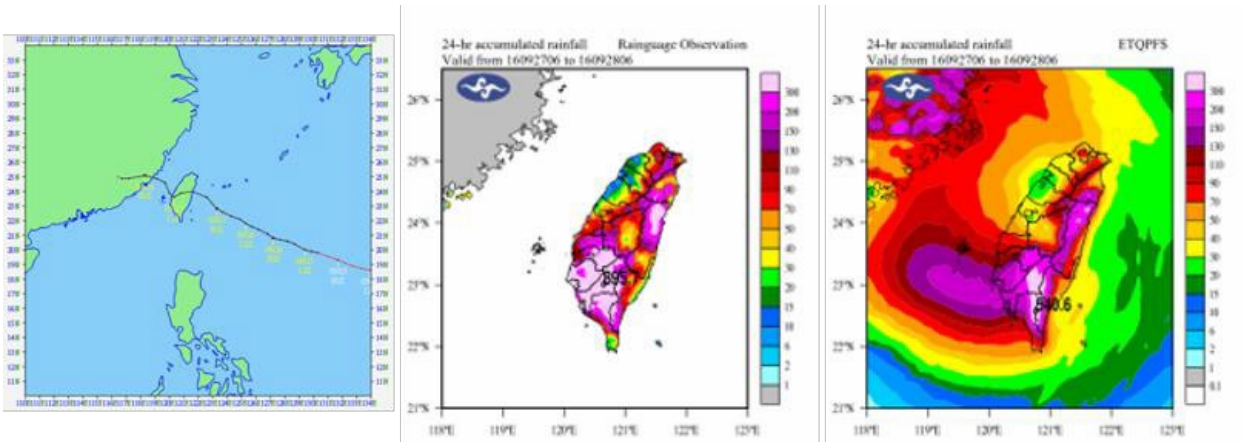

Fig. 10 (Left) The best track for Typhoon Megi (2016),(middle) The 24-h accumulated raingauge observation rainfall (mm; from 0600 UTC 27Sep to 0600 UTC 28Sep 2016),and (right) The 24-h accumulated ETQPF rainfall (mm; from 0600 UTC 27Sep to 0600 UTC 28Sep2016) (Hong et al. 2015).

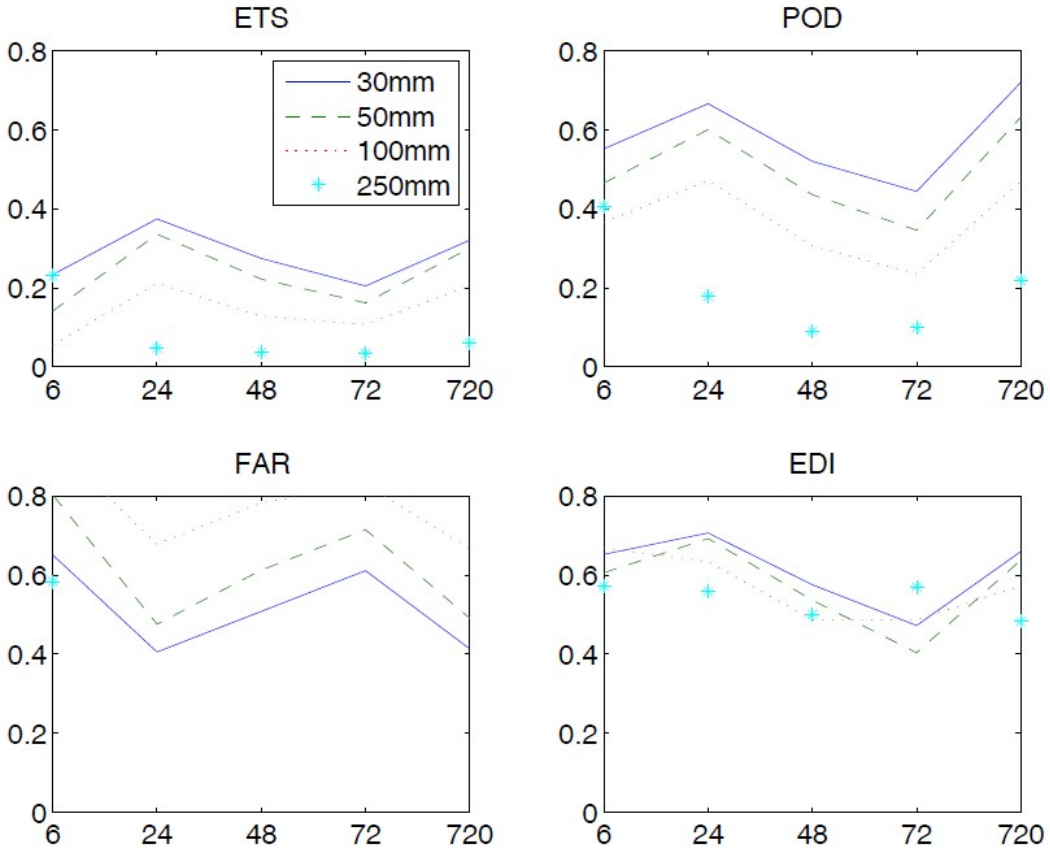

Fig. 11 Conventional verification results of ETS, POD, FAR, and EDI for 30, 50, 100, and 250mm rainfall thresholds. X-axis shows the accumulated rain forecast lead time of 0-6, 0-24, 24-48, 48-72, and 0-72 h, respectively. Y-axis shows the skill scores of the forecasts (Yu et al. 2018).

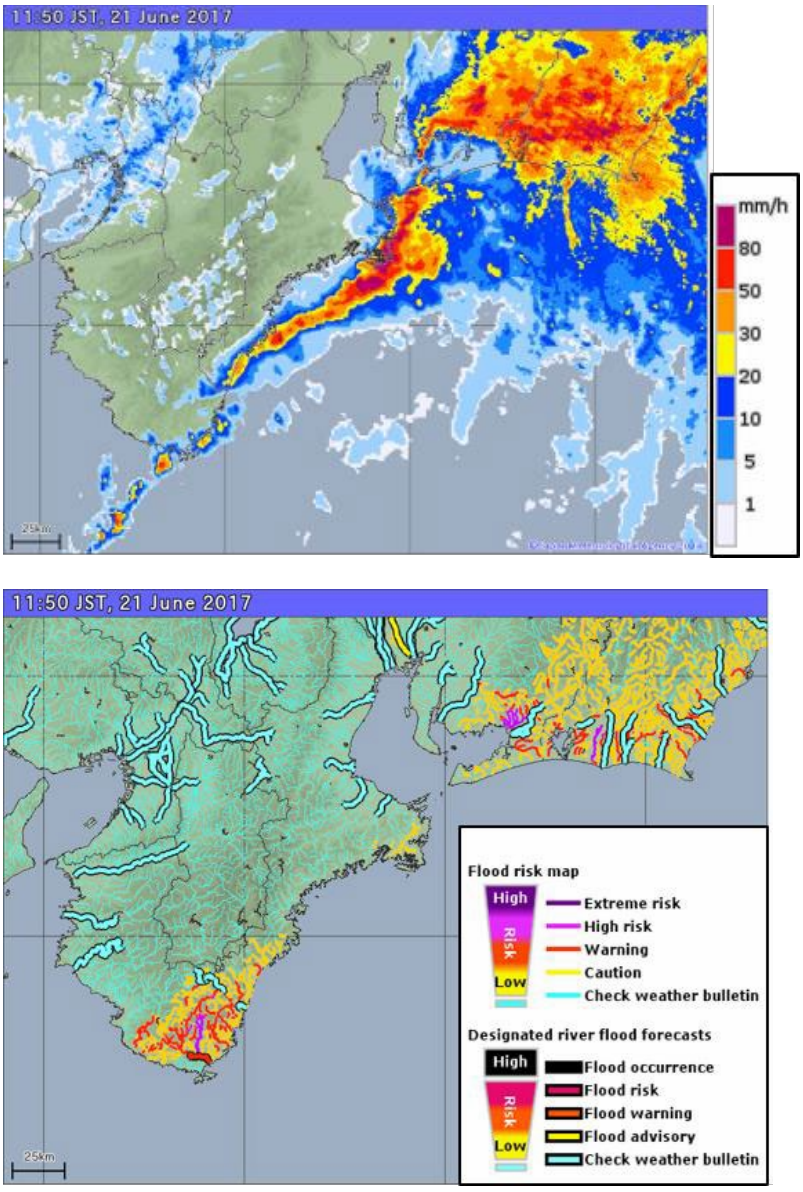

Fig. 12 An example of (upper) high-resolution precipitation nowcasting from the HRPNS and (lower) real-time flood risk distribution map (source: JMA).

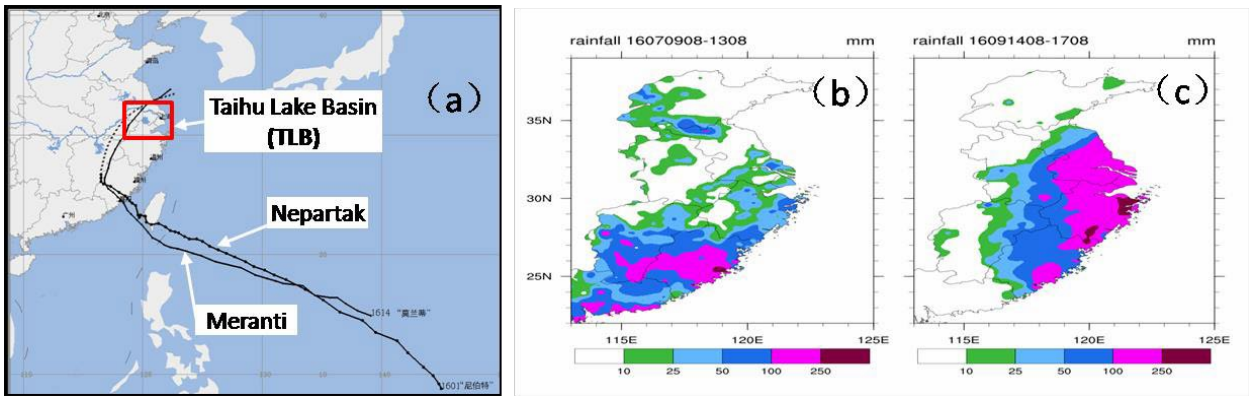

Fig. 13 (a) Track of Typhoon Nepartak and Meranti, the dashed line is track of Nepartak's remnant, the red box denotes the location of Taihu lake Basin (TLB). (b) Accumulated rainfall from 00UTC 9th to 00UTC 13th, July by Nepartak and its remnant. (c) Accumulated rainfall from 00UTC 14th to 00UTC 17th, Sep. by Meranti and its remnant (Shi et al. 2017b).

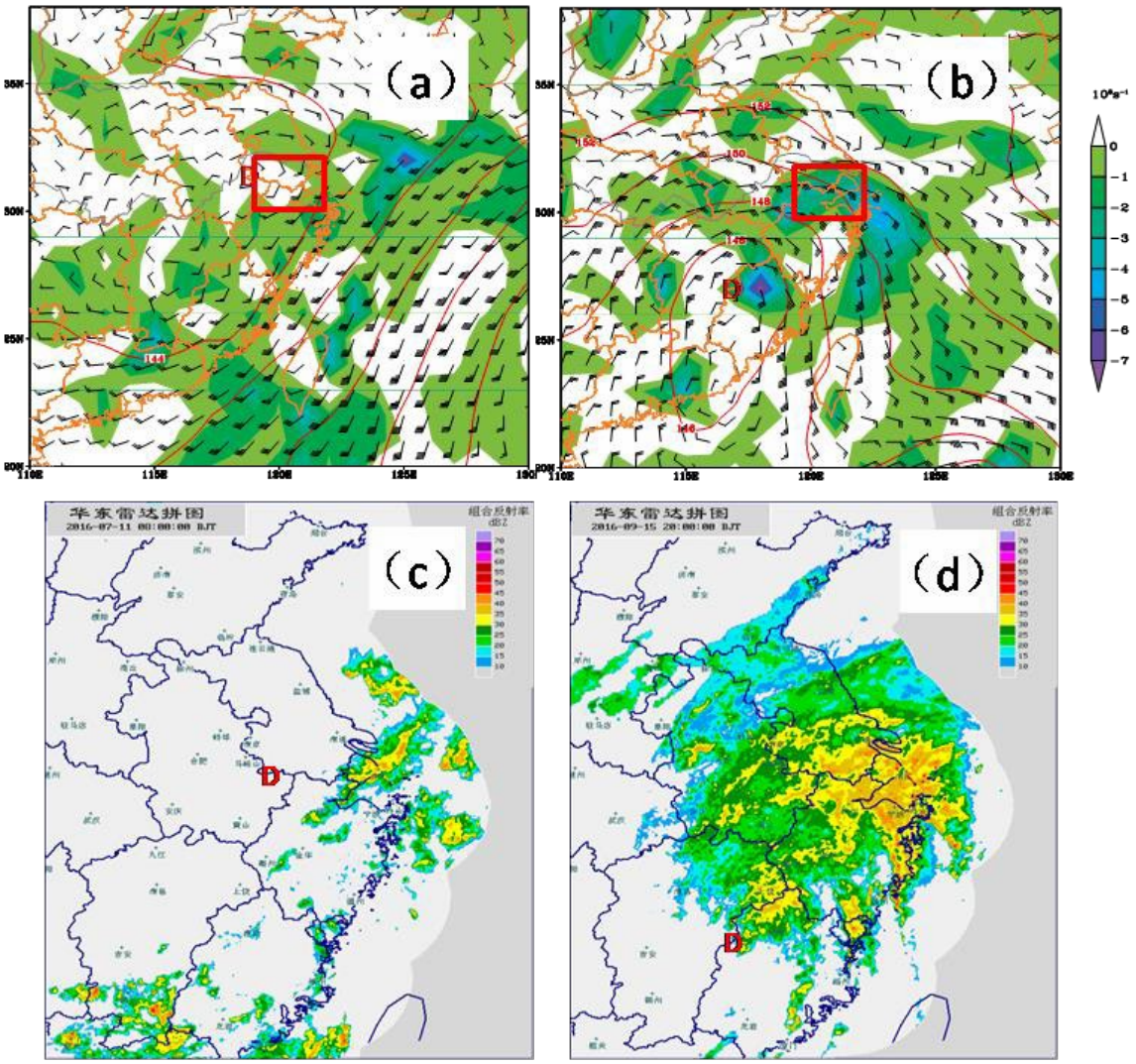

Fig. 14 (a) Reanalysis height, wind and vorticity fields of 850hPa at 00UTC 11th, July (Red 'D' denotes Nepartak's remnant center, the red box indicates the location of TLB). (b) Reanalysis height, wind and vorticity fields of 850hPa at 12UTC 15th, Sep. (Red 'D' denotes Meranti's remnant center, the red box indicates the location of TLB). (c) Radar reflectivity mosaic of east China at 00UTC 11th, July (Red 'D' denotes Nepartak's remnant center). (d) Radar reflectivity mosaic of east China at 12UTC 15th, Sep. (Red 'D' denotes Meranti's remnant center) (Shi et al. 2017b).

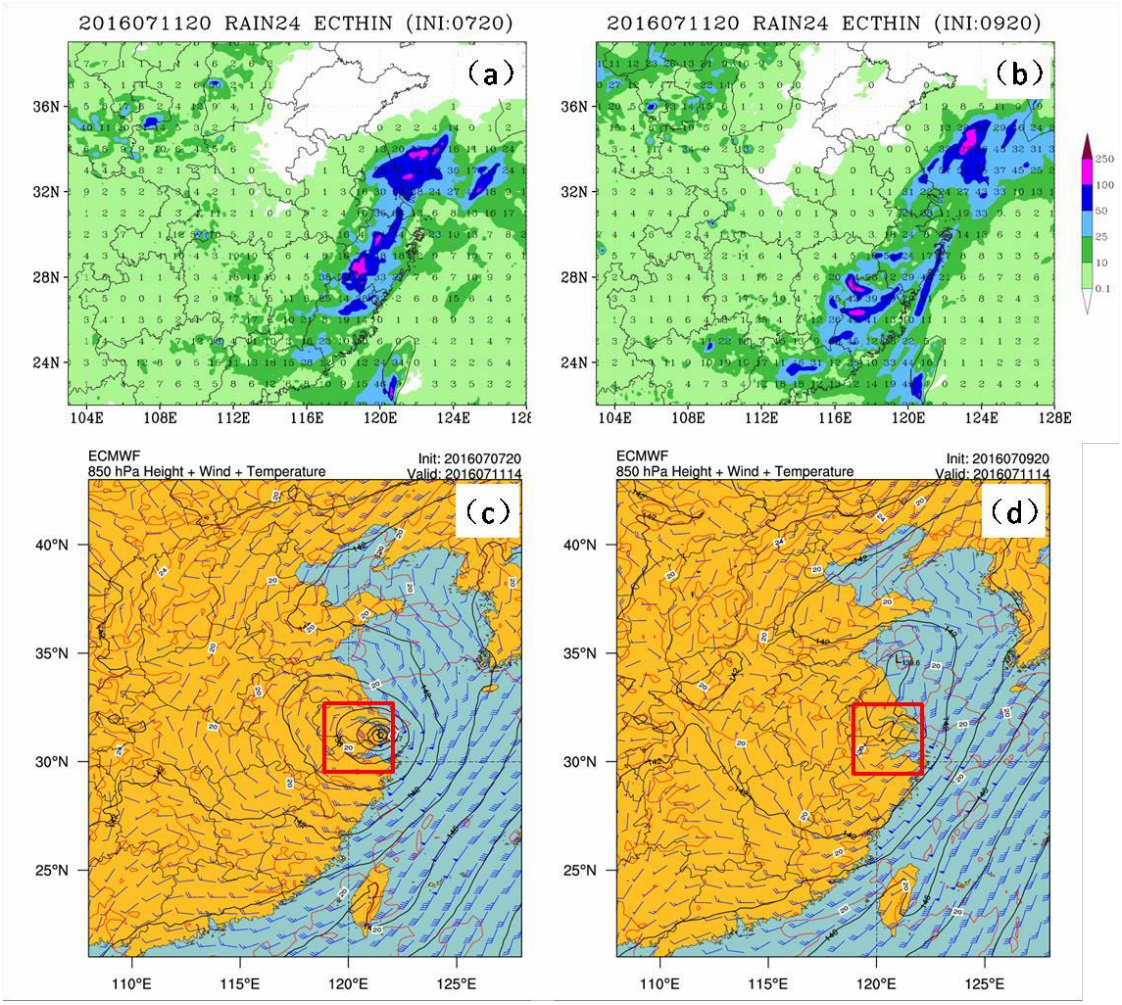

Fig. 15 (a) Rainfall forecast from 12UTC 10th to 12UTC 11th, July by ECMWF-IFS (initiated at 12UTC 7th, July). (b) Same as (a), but initiated at 12UTC 9th, July. (c) Height, wind and temperature fields at 06UTC 11th, July by ECMWF-IFS (initiated at 12UTC 7th, July; the red box indicates the location of TLB). (d) Same as (c), but initiated at 12UTC 9th, July (Shi et al. 2017).

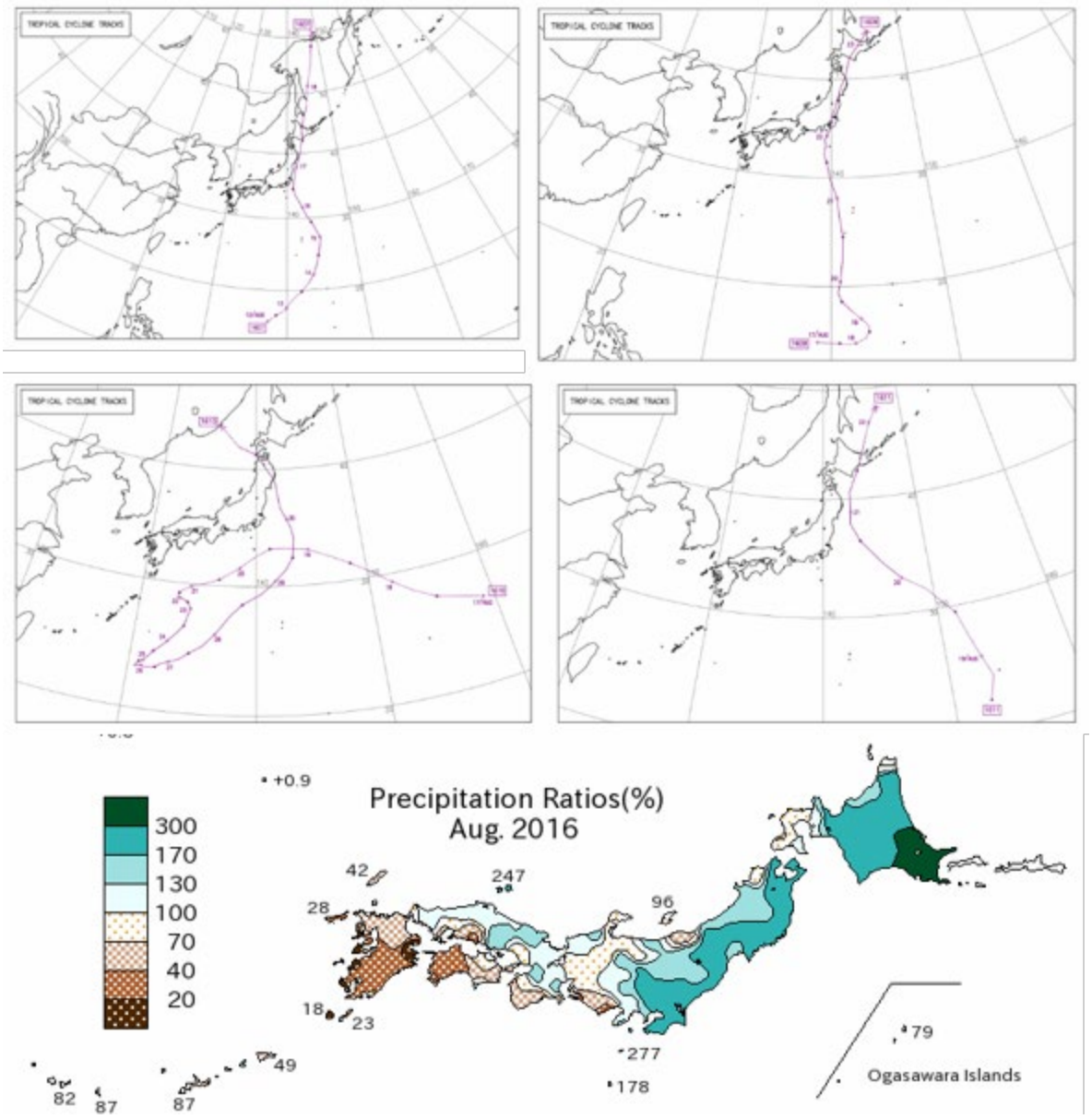

Fig. 16 The best tracks for typhoons Chanthu (upper left), Mindulle (upper right), Lionrock (middle left) and Kompasu (middle right). The four typhoons made landfall on the Pacific coast of northern Japan in a single month. (Lower) The monthly average precipitation ratio against normal for August 2016. The Pacific side of northern Japan experienced record-breaking monthly precipitation primarily due to typhoons (source: JMA).

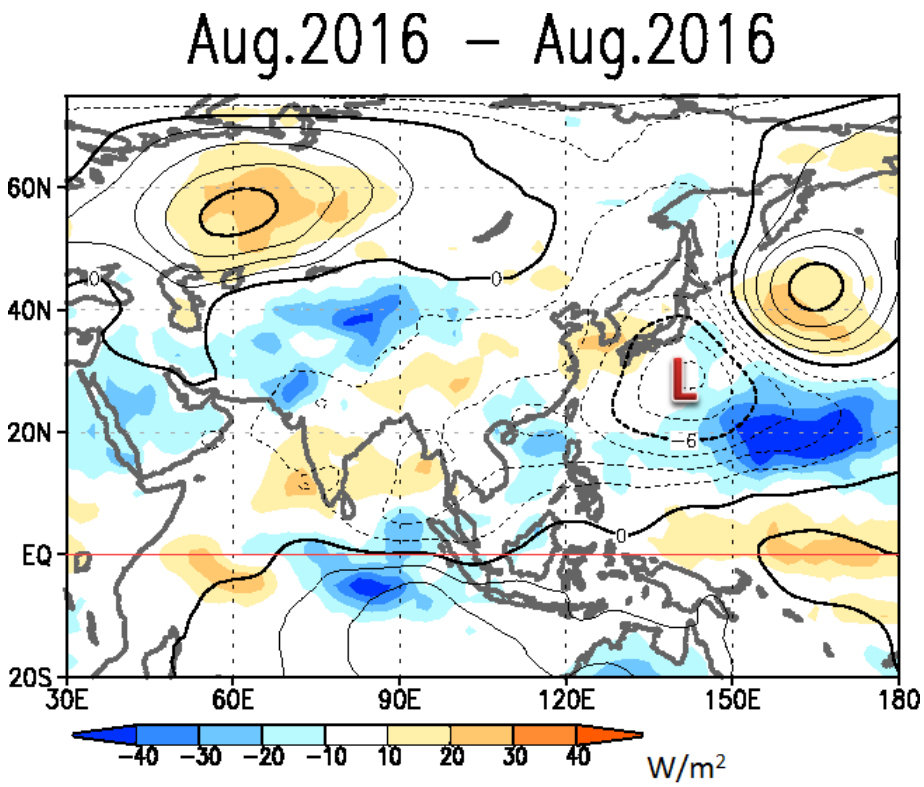

Fig. 17 Stream function anomalies at 850-hPa (contours) and outgoing longwave radiation anomalies (OLR; color shadings) for August 2016 (source: JMA).